LIQUID-SALT-COOLED REACTOR START-UP WITH NATURAL CIRCULATION UNDER LOSS-OF-OFFSITE-POWER (LOOP) CONDITIONS

A Thesis
Presented to
The Academic Faculty

by

Emilien B. Gros

In Partial Fulfillment
of the Requirements for the Degree
Master of Science in Nuclear Engineering

Georgia Institute of Technology
May 2012

LIQUID-SALT-COOLED REACTOR START-UP WITH NATURAL CIRCULATION UNDER LOSS-OF-OFFSITE-POWER (LOOP) CONDITIONS

Approved by:

Dr. B. Petrovic, Advisor
School of Mechanical Engineering
Georgia Institute of Technology

Dr. S. Duncan
School of Aerospace Engineering
Georgia Institute of Technology

Dr. S. Garimella
School of Mechanical Engineering
Georgia Institute of Technology

Dr. G. Yoder
Reactor and Nuclear Systems Division
Oak Ridge National Laboratory

Dr. D. Grgic
School of Electrical and Computer Engineering
University of Zagreb

Date Approved: December 06, 2011

ACKNOWLEDGEMENTS

Gratitude goes to my advisor, Dr. Bojan Petrovic, for his assistance, guidance, and support without which I could not have done this thesis.

I would like to thank my committee members, Dr. Scott Duncan, Dr. Srinivas Garimella, Dr. Graydon Yoder, and Dr. Davor Grgic for their time and help on this project.

I would also like to thank Andrew Bopp, for his contribution to my understanding of the RELAP5 code.

TABLE OF CONTENTS

LIST OF TABLES

LIST OF FIGURES

LIST OF SYMBOLS AND ABBREVIATIONS

LS-VHTR	Liquid-Salt-Cooled Very High-Temperature Reactor
LOOP	Loss Of Offsite Power
TRISO	TRiISOtopic
ORNL	Oak Ridge National Laboratory
ESBWR	Economic Simplified Boiling Water Reactor
BWR	Boiling Water Reactor
UCO	Uranium oxycarbide
UO2	Uranium dioxide
PyC	Pyrolytic Carbon
SiC	Silicon Carbide
VF	Volume Fraction
FLiBe	$LiF\text{-}BeF_2$
FLiNaK	LiF-NaF-KF
IHX	Intermediate Heat Exchanger
PB-AHTR	Pebble Bed Advanced High-Temperature Reactor
SCALE	Standardized Computer Analyses for Licensing Evaluation Modular Code System
RELAP	Reactor Excursion and Leak Analysis Program
INL	Idaho National Laboratory
LWR	Light Water Reactors
RVACS	Reactor Vessel Auxiliary Cooling System
DRACS	Direct Decay Heat Removal System
PRACS	Passive Decay Heat Removal System

SUMMARY

The Liquid-Salt-Cooled Very High-Temperature Reactor (LS-VHTR) was modeled using the neutronics analysis code SCALE6.0 and the thermal-hydraulics and kinetics modeling code RELAP5-3D with objective to devise, analyze, and evaluate the feasibility and stability of a start-up procedure for this reactor using natural circulation of the coolant and under the Loss Of Offsite Power (LOOP) conditions.

This Generation IV reactor design has been studied by research facilities worldwide for almost a decade. While neutronics and thermal-hydraulics analyses have been previously performed to show the performance of the reactor during normal operation and for shutdown scenarios, no study has heretofore been published to examine the active or passive start-up of the reactor.

The fuel temperature (Doppler) and coolant density coefficient of reactivity of the LS-VHTR were examined using the CSAS6 module of the SCALE6.0 code. Negative Doppler and coolant density feedback coefficients were calculated.

Two initial RELAP5 simulations were run to obtain the steady-state conditions of the model and to predict the changes of the thermal-hydraulic parameters during the shutdown of the reactor. Next, a series of step reactivity additions to the core were simulated to determine how much reactivity can be inserted without jeopardizing safety and the stability of the core. Finally, a start-up procedure was developed, and the restart of the reactor with natural convection of the coolant was simulated. The results of the simulations demonstrated the potential of a passive start-up of the LS-VHTR.

CHAPTER 1

INTRODUCTION

The Liquid-Salt-Cooled Very High-Temperature Reactor (LS-VHTR) is one of the six concepts of Generation IV reactors [1]. It has conceptually many promising features and combines several new technology assets such as: the use of the TRiISOtopic (TRISO) fuel particles, high operating temperatures (> 750°C), Brayton power conversion cycle, passive safety systems and a low pressure liquid-salt coolant. The LS-VHTR project goal is to provide an advanced design which offers the potential for higher power output, improved efficiency of electricity production, and higher operating temperatures leading to significant reduction in plant capital costs, as well as its use in high-temperature process heat applications. This concept of reactors is under study in research facilities worldwide. In particular, Oak Ridge National Laboratory (ORNL) has been conducting research on the LS-VHTR for almost a decade and has developed a baseline design for a 2400 MWth plant that was used in this study [2].

Regulations for current nuclear power plants demand that a nuclear power plant have redundant safety features. In most nuclear reactor designs, there are two connections to the electrical grid. In case of a LOOP, during a blackout for instance, the plant loses a connection, and may have to be tripped for safety reasons. After a power outage, since nuclear power plants require re-establishing the two connections and a large amount of energy to be started-up, they are usually the last power stations to be brought back on-line, leading to significant economic losses.

Therefore, the purpose of this thesis is to evaluate the feasibility and stability of a start-up process for the LS-VHTR with natural circulation of the coolant. This novel concept for the start-up of a nuclear plant of LS-VHTR type would enable the restart of the plant under LOOP conditions, which would then help to restore the grid. Indeed, the

use of natural convection suppresses the need for pumps during the start-up, thus minimizing the amount of electricity required.

Since commercial nuclear energy started in the mid 1950s, almost all of the reactors have been using forced convection to drive the coolant flow. Limited experience on start-up and operation under natural circulation of the coolant comes from the Dodewaard nuclear power plant, that was operated in the Netherlands until 1997, with a net output of 55 MWe [3], and from the passively safe generation III+ reactor ESBWR (Economic Simplified Boiling Water Reactor) designed by GE Hitachi Nuclear Energy that is waiting for final design certification [4]. However, the Dodewaard reactor and the ESBWR are Boiling Water Reactors (BWRs), thus physics phenomena are different than in the LS-VHTR.

Computational models have been developed and initially used to evaluate and analyze the performance of the LS-VHTR during normal operation and for shutdown scenarios. In this study, we used a neutronics analysis code: SCALE6.0 [5], a thermal-hydraulics and kinetics modeling code: RELAP5 [6], and other simulation approaches to model and analyze the behavior of the reactor during start-up with natural circulation of the salt coolant.

Natural convection provides several advantages, such as the elimination of the need for pumps, improved safety and system simplification. Though natural circulation of the coolant may lead to instabilities, low driving forces or low mass fluxes. Thus, it is essential to specify a procedure for the start-up of the LS-VHTR using natural circulation and to study its stability during that transient.

The SCALE6 code was used to model the core and to calculate the fuel temperature coefficient of reactivity (Doppler coefficient) as well as the coolant density reactivity coefficient of the reactor. These coefficients were used as inputs for the RELAP5 code. The latter was used to simulate the start-up procedure and provide mass

flow rate, power, temperature, reactivity profiles and other relevant parameter values during the transient.

The following chapters present the work performed. Chapter II provides an overview of the LS-VHTR core and power plant design. A literature review focusing on natural circulation, reactivity control and start-up process is presented in Chapter III. Chapter IV describes the methodology, models and software used. It should be noted that modeling this type of reactor is in its infancy, and developing the models themselves is a novel contribution. The results of the simulation are presented and analyzed in Chapter V. Finally, Chapter VI summarizes the outcome of this study and includes suggestions for further work.

CHAPTER 2

REACTOR CORE AND NUCLEAR POWER PLANT DESIGN

The LS-VHTR represents a unique merging of several design features. In this chapter, the specificities of the design chosen are presented.

2.1 Configuration and dimensions

A functional diagram of the LS-VHTR layout is shown in Figure 2.1. The core and the primary heat exchanger are located in a large pool containing a buffer salt. The heat generated by the fuel is removed by a liquid-salt coolant flowing upwards in the core. This fluid flows in a primary loop through the primary heat exchanger, where heat is transferred to an intermediate loop containing another salt. The primary loop is closed and immersed in the buffer salt tank. The salt in the secondary loop conveys heat to a second heat exchanger, where helium flowing in a third loop is heated. This helium, once heated, flows through turbines in order to produce electricity. Alternatively, supercritical CO_2 or supercritical steam may be used. In this thesis, the core, the primary loop, the primary heat exchanger and part of the intermediate loop were modeled. Thus, we will not develop the design of the passive decay heat removal systems and the Brayton electricity production process.

Figure 2.2 shows a cross sectional view of the reactor. The 12 m tall core is composed of 8 m of active fuel, a lower plenum, lower reflector, upper reflector, and upper plenum of 1 m height each. The core diameter (including fuel assemblies and outer reflector blocks) is 9.2 m.

During normal operation, the pump located above the reactor core drives the flow in the primary loop. Similarly, a second pump drives the flow of salt in the secondary loop and a circulator is used in the power conversion loop (helium).

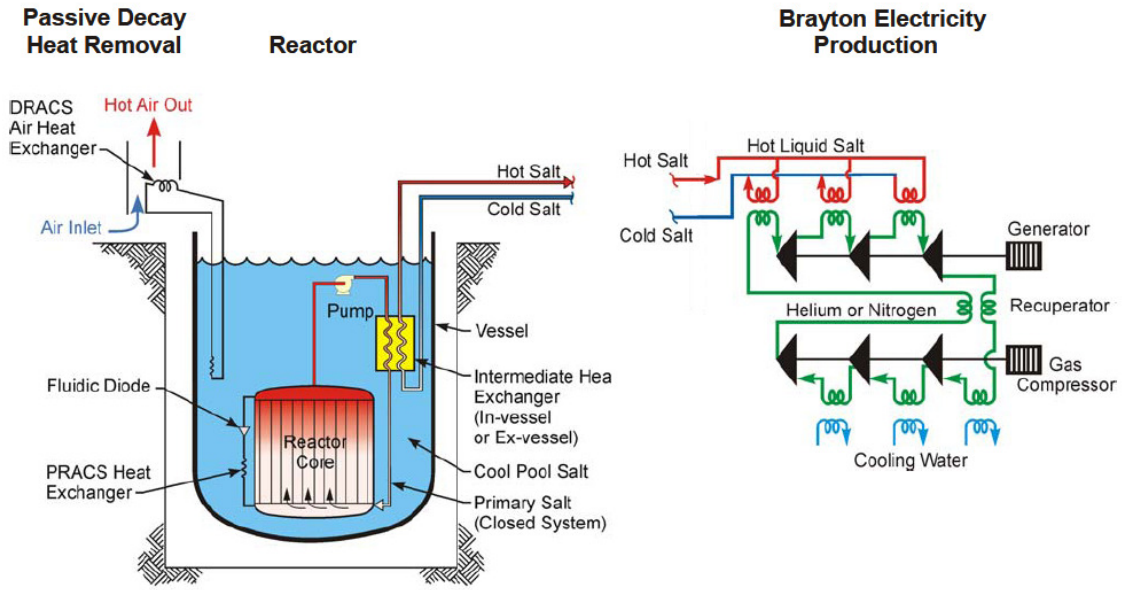

Figure 2.1: Configuration of the LS-VHTR plant [7]

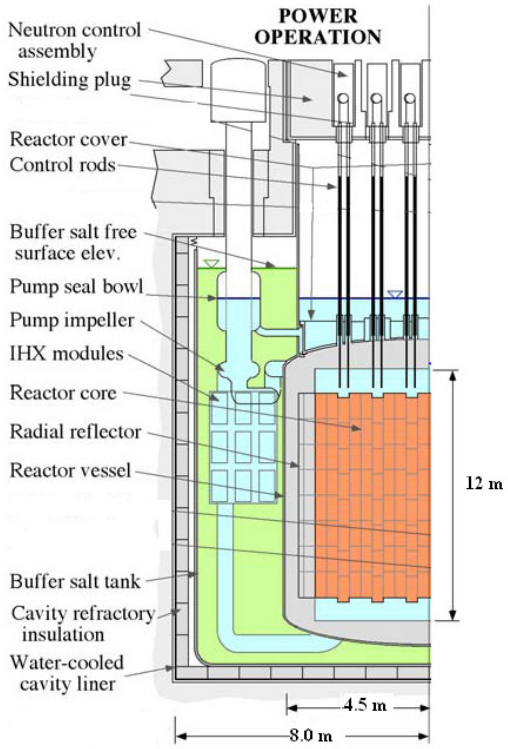

Figure 2.2: Elevation view of the LS-VHTR [7]

2.2 Fuel element, fuel assembly and fuel core design

The LS-VHTR uses TRISO (TRiISOtopic) fuel particles, which were developed for use in various high temperature reactor concepts. It consists of a fuel kernel made of uranium oxycarbide (UCO) or uranium dioxide (UO_2), surrounded by four different layers of carbon composites. The first layer is a porous carbon layer designed to absorb fission product gases and allow room for irradiation-induced expansion of the fuel kernel. The second layer, made of Pyrolytic Carbon (PyC), protects the next layer from the recoil of fission products and aids in transporting the fission heat energy out of the particle. The Silicon Carbide (SiC) layer serves as the "pressure vessel" that contains the fission products [8]. The outer Pyrolytic Carbon layer compresses the SiC layer during irradiation and provides a bonding surface for matrix material during fuel fabrication. Figure 2.3 illustrates the configuration of the various layers of the TRISO particle.

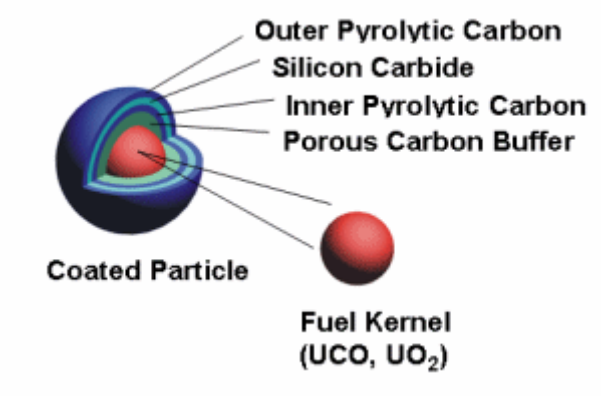

Figure 2.3: TRISO fuel particle [9]

The TRISO particles are placed in a graphite moderating matrix of density 1.74 g/cm^3 and compressed into a cylindrical carbon compact. The ratio of the volume of TRISO particles to the volume of moderating material in the compact is called the volume fraction (VF). These compacts are then stacked in the fuel channels of the fuel assembly.

The prismatic block fuel assembly option was chosen for this design. A single fuel block is shown in Figure 2.4. It has a flat-to-flat dimension of 36 cm, is 79.3 cm high, and is made of graphite. One fuel block consists of 216 fuel channels (1.27 cm diameter) and 108 coolant channels (0.953 cm diameter). The fuel and coolant channels are arranged in a triangular array. The distance between two channels is 1.9 cm. There is a fuel handling hole located at the center of the block that allows the assembly to be removed from the core. This fuel block configuration option follows the FY-2004 baseline design developed by ORNL [2]. A fuel assembly is made of 10 of these fuel blocks stacked axially together, thus the fuel assembly height is 7.93 m.

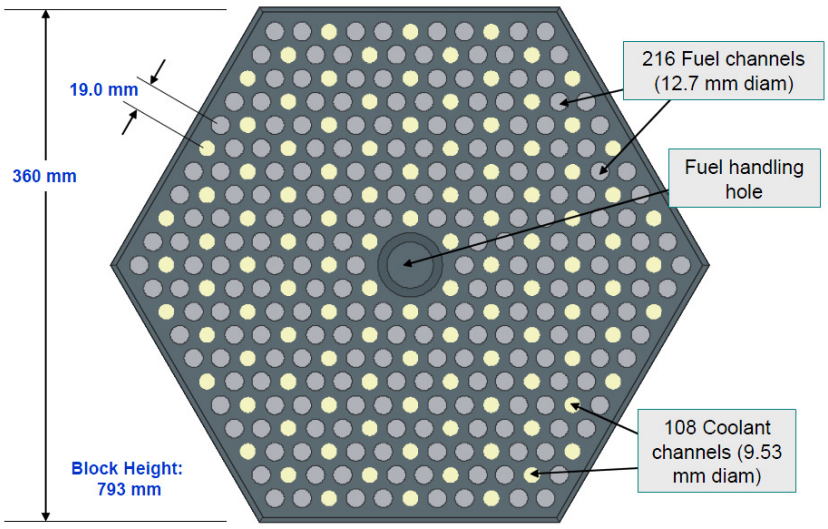

Figure 2.4: LS-VHTR hexagonal fuel assembly block [2]

The reactor core design is shown in Figure 2.5. The core is 8 m tall and has a diameter of 9 m. It consists of 265 fuel assemblies arranged so that they form a fuel region surrounded by four rows of reflector blocks. The latter have the same dimensions as the fuel blocks, and are composed of graphite. This reactor core configuration is identical as that of the FY-2005 ORNL design [10].

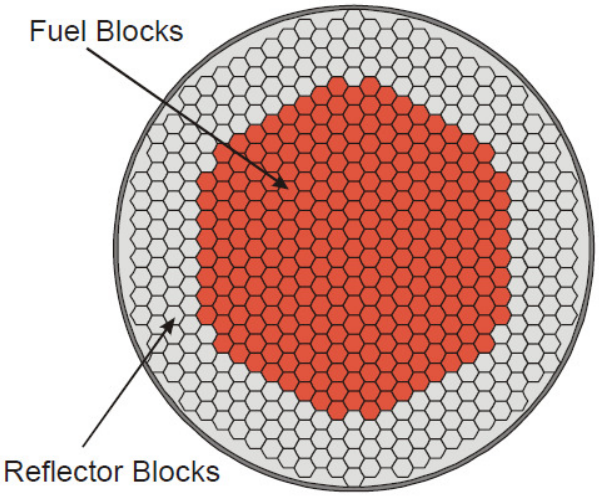

Figure 2.5: LS-VHTR reactor core design [10]

The main parameters for the fuel assembly specified in the 2004 ORNL design of the LS-VHTR are listed in Table 2.1.

Table 2.1: ORNL specifications for the reactor fuel assembly model [2]

Coated fuel particle	Fuel : UO_2, 10.4 g/cm^3, 10.36 wt% ^{235}U
	Fuel kernel: 350 µm diameter
	1st coating: carbon buffer, 100 µm thickness, 1.0 g/cm^3
	2nd coating: inner pyrolitic carbon, 35 µm thickness, 1.85 g/cm^3
	3rd coating: SiC, 35 µm thickness, 3.20 g/cm^3
	4th coating: outer pyrolitic carbon, 40 µm thickness, 1.80 g/cm^3
Fuel Compact	Diameter: 1.25 cm
	Length: 5.3 cm
	Standard fuel element: 1.60 g U per compact
	Number of compacts per fuel hole: 15
	Fuel compact graphite matrix: 1.74 g/cm^3
Fuel assembly	Hexagonal, width across flats: 36.0 cm
	Graphite density: 1.74 g/cm^3
	Height: 79.5 cm
	Standard fuel elements per column: 10
	Fuel rod channel diameter: 1.27 cm
	Number fuel rod channels per element: 216
	Coolant channel diameter: 0.95 cm
	Number coolant channels per element: 108
	Pitch between channels: 1.90 cm

2.3 Salt choice

There are several salts under consideration for use in the LS-VHTR such as: LiF-BeF_2 (FLiBe), $NaFBeF_2$, LiF-NaF-KF (FLiNaK), or NaF-ZrF_4 [7]. Salts are used for heat transport in this reactor. They are characterized by low melting point, high boiling point, good heat transfer capabilities, and they enable the reactor to be operated at high temperatures. These characteristics lead to greater power efficiencies. Based on heat transfer characteristics, material compatibility, freezing temperature, attractive neutronics, cost and other criteria, FLiBe is usually preferred to other candidates to be the primary salt [10]. Table 2.2 presents the thermophysical properties of several reactor coolants. FLiNaK is considered as a good candidate for the intermediate loop [7], and was arbitrarily chosen as the intermediate salt in this study. The main differences between the two salts are the neutron absorption cross section and the cost.

Table 2.2: Properties of molten salts and common reactor coolants [11]

Coolants	Heat capacity Cp (cal/g-°C)	Density ρ (g/cc)	Viscosity μ (cP)	Volume expansivity β (1/°C)	Thermal conductivity k (W/m-K)	Prandtl # Cp*μ/k
Comparison coolants						
Water (300°C)	1.370	0.72	0.09	3.30E-03	0.54	0.967
Na (550°C)	0.303	0.82	0.23	8.60E-04	62	0.004
NaF-$NaBF_4$ (700°C)	0.360	1.75	0.88	4.25E-04	0.5	2.640
Candidate salt coolants at 700°C						
FLiNaK	0.450	2.02	2.9	3.61E-04	0.92	5.938
LiF-NaF-RbF	0.236	2.69	2.6	3.01E-04	0.62	4.143
2LiF-BeF_2	0.577	1.94	5.6	2.52E-04	1	13.525
NaF-BeF_2	0.520	2.01	7	1.84E-04	0.87	17.513
LiF-NaF-BeF_2	0.489	2.00	5	2.25E-04	0.97	10.551
LiF-ZrF_4	0.292	3.09	> 5.2	2.99E-04	0.48	> 13.241
NaF-ZrF_4	0.280	3.14	5.1	2.96E-04	0.49	12.199
KF-ZrF_4	0.251	2.80	< 5.1	3.17E-04	0.45	< 11.907
RbF-ZrF_4	0.200	3.22	5.1	3.11E-04	0.39	10.948
LiF-NaF-ZrF_4	0.300	2.79	6.9	3.12E-04	0.53	19.073

2.3.1 Primary salt: FLiBe

For the primary loop, FLiBe was the prime candidate because of its very high volumetric heat capacity as well as its stability above 800°C and under intense radiation. FLiBe is a compound of LiF (66%) and BeF_2 (34%). It has a relatively low neutron absorption cross section. FLiBe salt shows great performance under activation. It does not generate gamma activity for more than one minute past being activated. Finally, the melting temperature of FLiBe is 459°C, and its boiling temperature is 1430°C [12].

However, FLiBe requires a high concentration of ^{7}Li (99.99%), which requires isotopic enrichment and may lead to some problems in mass production [2]. Also, the cost of this salt is higher than that of the other candidates: $52.2 /l [11]. However, this high cost is compensated by the neutronic and thermal performances of the salt.

2.3.2 Secondary salt: FLiNaK

FLiNaK is a compound of LiF (46.5%), NaF (11.5%) and KF (42%). It has a similar freezing point as FLiBe, but a lower heat capacity, lower thermal conductivity, and higher neutron absorption cross section. The melting and boiling temperature of FLiNaK are 454°C and 1570°C respectively [13]. FLiNaK is also twice as cheap as FLiBe: $24.1 /l [11]. Its reduced price compared to FLiBe and its high freezing point make it a prime candidate for the secondary salt.

2.4 Intermediate heat exchanger design

The intermediate heat exchanger (IHX) transfers heat from the primary salt to the secondary salt. Several types of heat exchangers; compact plate types and shell-and tube types, were considered for use in the LS-VHTR as the IHX [2] [14]. To facilitate in-service inspection and reliability, as well as RELAP5 modeling, it was decided to use the shell-and-tube type for the IHX design in this study. A conceptual design of the IHX for another type of LS-VHTR, the Pebble Bed Advanced High-Temperature Reactor (PB-

AHTR), was developed at the U.C. Berkeley [15]. Given that this study focuses on the core and primary coolant performance, it was decided to pick parameters for the IHX using the conceptual design developed at UCB and recommendations made by ORNL. RELAP5 simulations of the reactor operating at full power conditions showed that the IHX as modeled is capable of transferring all of the heat generated in the core to the intermediate loop. Figure 2.6 illustrates the simple (one pass tube-side) shell-and-tube heat exchanger design chosen for the IHX in this study. The parameters used to model the IHX are shown in Table 2.3.

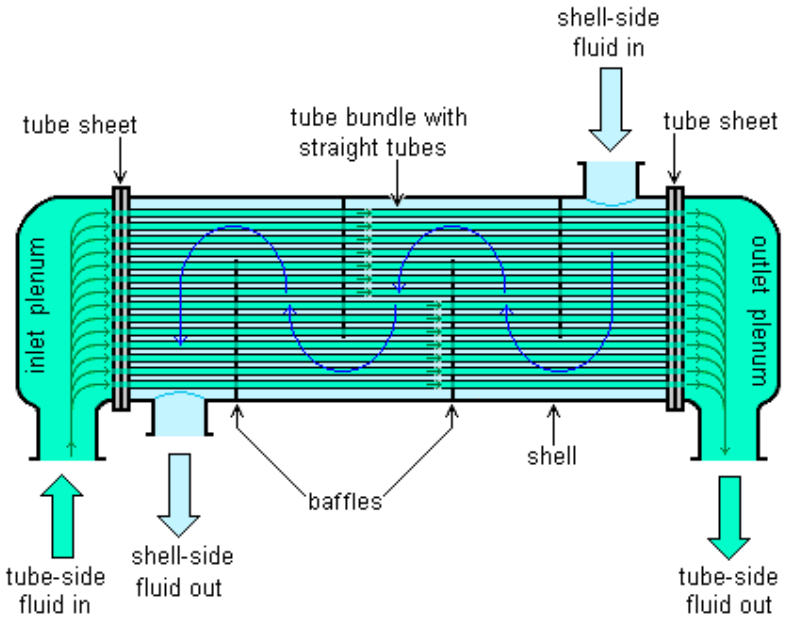

Figure 2.6: Straight-tube shell-and-tube type heat exchanger [16]

Table 2.3: Main parameters of the IHX used in this study

Type	Shell-and-tube
Primary salt	FLiBe
Secondary salt	FLiNaK
Tube material	Hastelloy N
Outside diameter of tubes (cm)	0.95
Wall thickness of tubes (cm)	0.13
Total tube length (m)	8.0
Total number of tubes	11250.0
IHX diameter (m)	1.24

2.5 Nuclear power plant main parameters

The main parameters of the LS-VHTR under study including electrical and thermal power performance, temperature, pressure and mass flow rate in the primary and intermediate loop are given in Table 2.4. It should be noted that the value for the intermediate loop flow rate was found in units of m^3/s [2]. It was converted into kg/s using FLiNaK density at 1193 K: 1840 kg/m^3 [17].

Table 2.4: Main parameters of the LS-VHTR power plant [2]

Thermal power (MW)	2400
Electrical power (MW)	1300
Primary loop maximum temperature (K)	1273
Core pressure drop (MPa)	0.129
Primary loop net mass flow rate (kg/s)	10000
Intermediate loop maximum temperature (K)	1193
Intermediate loop minimum temperature (K)	1133
Intermediate loop mass flow rate (kg/s)	16400
Overall cycle efficiency	0.54

CHAPTER 3

THEORY AND LITERATURE REVIEW

3.1 Natural circulation review

3.1.1 Natural circulation properties and equations

The flow of a fluid under natural circulation is driven by natural forces such as convection and gravity. Figure 3.1 illustrates the principle of natural circulation with a simple uniform rectangular loop with adiabatic pipes, a heat sink and a heat source.

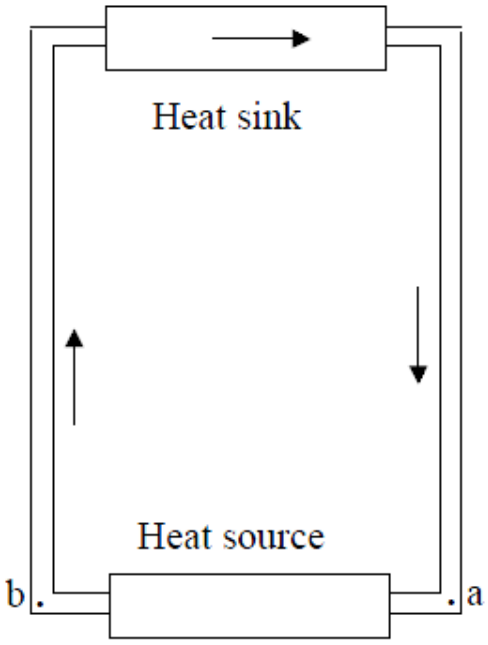

Figure 3.1: A simple natural circulation system [18]

As the fluid flows through the source, heat is transferred to it, leading to a decrease of the fluid density. On the contrary, the fluid density increases while the fluid flows through the heat sink. These changes in density lead to a pressure difference between points “a” and “b” which causes the natural circulation flow.

In the primary loop of the LS-VHTR under study, the heat source is the core that generates heat, which is transferred to the coolant channels, while the heat sink is the intermediate heat exchanger, transferring heat from FLiBe to FLiNaK.

The use of natural convection of the reactor coolant eliminates the need for using circulating pumps during start-up, thus reducing the amount of offsite power needed. This is also a safety asset since it eliminates the risks of pump failures during start-up. Moreover, using natural convection of the coolant during start-up increases design safety integrity and reliability. Given that this study aims at evaluating a start-up procedure for the LS-VHTR that would minimize the need for external power, natural circulation of the coolant was used.

There are also several drawbacks associated with naturally driven flows, such that it leads to low driving forces or low mass fluxes. Also, using natural circulation during the start-up of the reactor or for normal operation may lead to instabilities. Thus, the specification of start-up and operating procedures may be complex. Finally, to enhance natural convection flow rates, it is necessary to minimize pressure losses by eliminating all unnecessary pipe bends, elbows, etc. Thus, natural circulation systems tend to be simpler than forced convection ones. This may be an advantage (simplicity of the piping layout is a safety and a manufacturing asset) or a drawback (lack of flexibility; designers have to make trade-offs to strike a balance between flexibility and simplicity [18]).

3.1.2 Operating experience on natural circulation

Natural circulation operation has been tested on integral system test facilities and on a few small sized nuclear power reactors like the S5G and S8G United States Naval reactors, the Russian VK-50 nuclear reactor, the US Humbolt Bay Boiling Water Reactor (BWR) or the Dodewaard plant in the Netherlands. The ESBWR designed by GE Hitachi is also aiming at using natural convection of water during start-up and normal operation.

In the following paragraphs, the design and start-up procedures of the Dodewaard plant and of the ESBWR will be described.

3.1.2.1 Experience from the Dodewaard plant operation

The Dodewaard nuclear reactor is a 183 MWth natural circulation BWR/1 that was built in the Netherlands and operated from October 1968 until 1997, when it was shut down for economic reasons [3]. Several stability tests have been run and no unstable oscillations during the course of start-up have been observed during the plant operating history. Figure 3.2 provides a flow diagram of the plant; solid lines represent the liquid water flow while dashed lines represent steam.

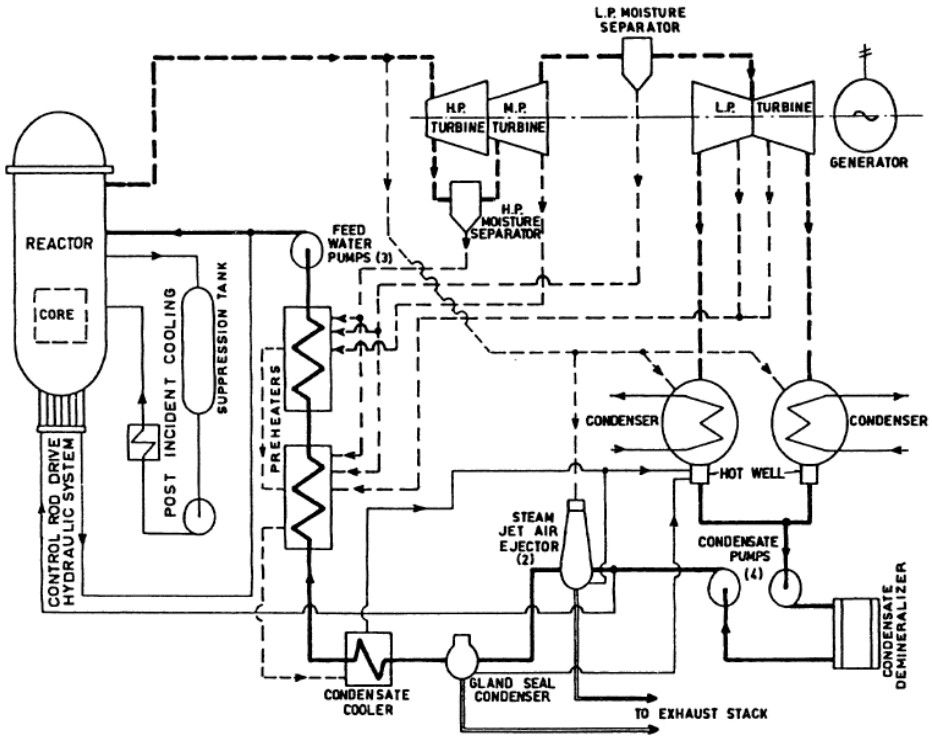

Figure 3.2: Dodewaard plant flow diagram [19]

The reactor start-up procedure for the Dodewaard plant is as follows. “Cold start-up is initiated at a refueling water temperature of approximately 60°C. The initial coolant

heat up is done using the reactor shutdown cooling system and decay power. When the coolant reaches saturation conditions of 100°C the reactor is brought to critical conditions; the power and pressure are then slowly increased to full load conditions. Reactor heat up rate is then controlled at rate of 45 to 55°C per hour with the control rod system [19]". In this study, we try to establish a similar start-up procedure for the LS-VHTR. Thermal stratification (i.e. cold water accumulates in the plenum region and hot water accumulates in the core region) was identified as one potential instability issue for the start-up, since sudden entrainment of cold water due to recirculation flow at the onset of core boiling might trigger unstable power and flow oscillations. This may not be a concern for the LS-VHTR under natural circulation start-up since the operating temperature prevents the salt coolant from boiling.

3.1.2.2 ESBWR design and start-up procedure

The ESBWR is a 4500 MWth reactor designed by GE Hitachi Nuclear Energy [20]. Figure 3.3 shows a cross-sectional view of the ESBWR reactor vessel. Cold feedwater is injected in the core region, heated up until boiling while it flows upward through the core, and steam flows out of the upper plenum at the top of the core. The flow is dependent on the differential water level (about 8.2 m) and loop pressure drops. There are no recirculation pumps and none of the associated power supplies, and the ESBWR is designed so that natural convection of water is used during start-up and full power conditions.

Reactor initial coolant heat-up is performed using decay heat and auxiliary heating systems (auxiliary boilers). This means that outside power is needed to start-up the ESBWR. The start-up procedure of the ESBWR is similar to that of the Dodewaard plant start-up, and is as follows. Water coolant is heated up to about 85°C, while it is deaerated. Control rods are withdrawn to reach criticality, and then the power increase is

controlled and maintained at a certain rate. Pressure is controlled by turbine bypass valves.

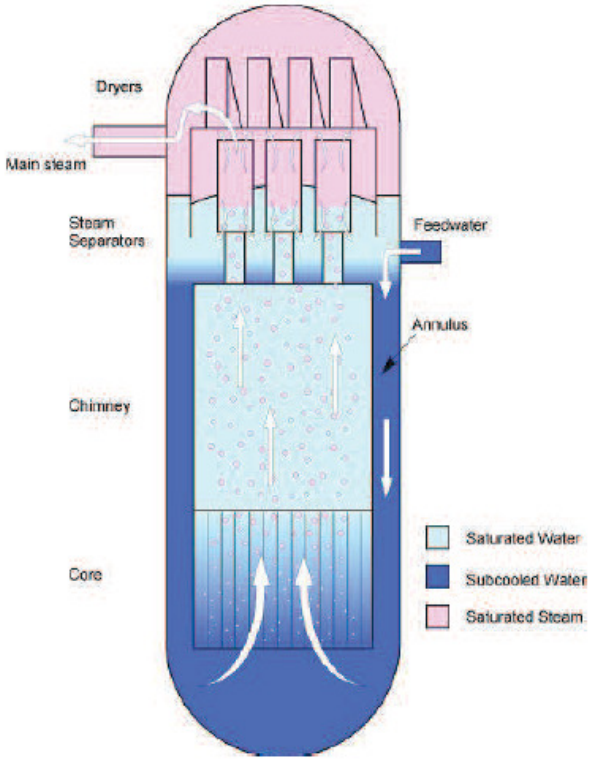

Figure 3.3: Cross-sectional view of the ESBWR vessel [21]

The following graphs provide an overview of the ESBWR start-up. Figure 3.4, 3.5 and 3.6 are results from TRACG (a GE proprietary version of the Transient Reactor Analysis Code (TRAC) code used for the analysis of ESBWR stability margins) simulations and show respectively the total core power, hot bundle inlet subcooling and total core flow of the ESBWR during the start-up transient.

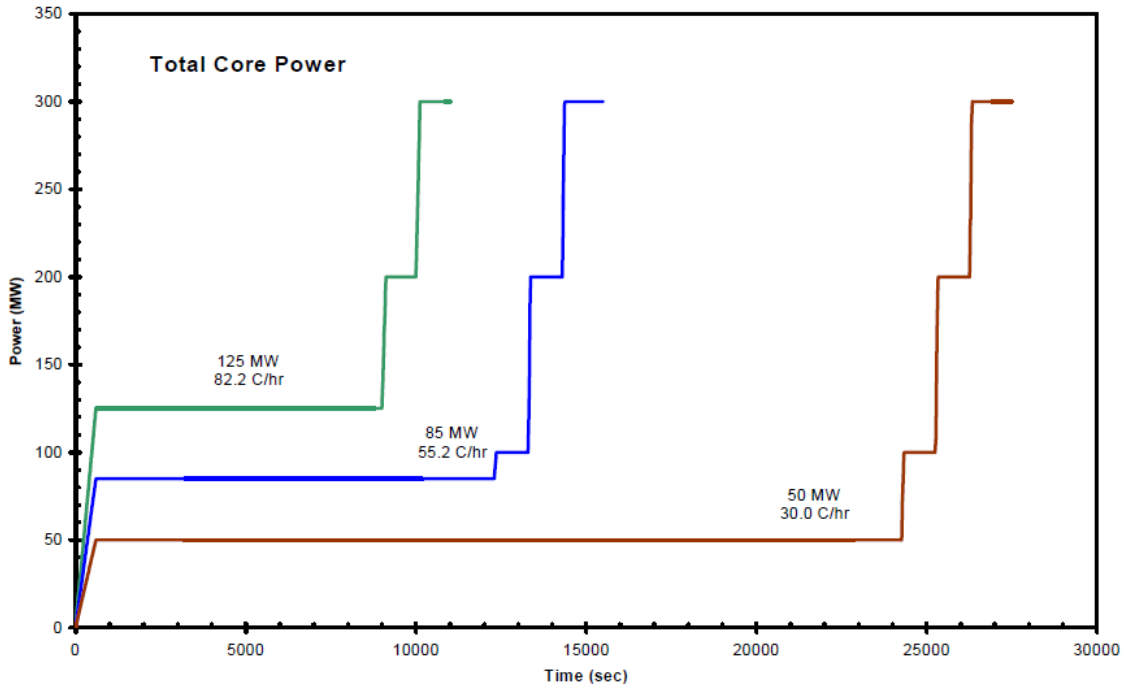

Figure 3.4: Total ESBWR core power during start-up [22]

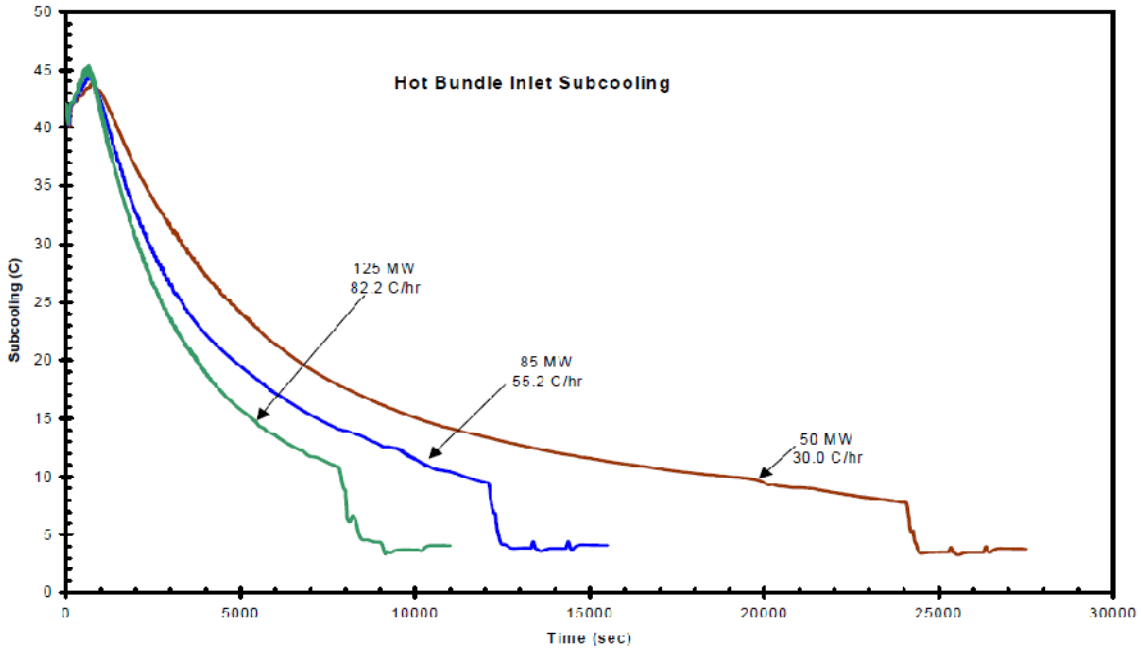

Figure 3.5: Hot bundle inlet subcooling during start-up [22]

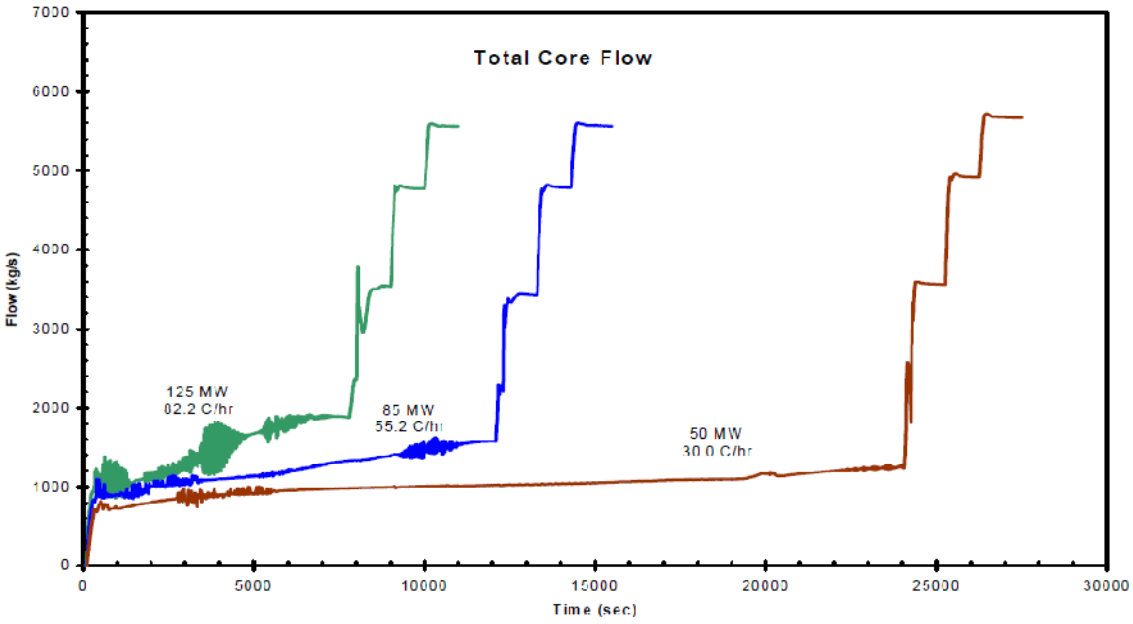

Figure 3.6: Total core flow during start-up [22]

3.2 Nuclear reactor kinetics

3.2.1 The point reactor kinetics model

The reactivity of the core is defined as:

$$\rho(t) = \frac{(k(t) - 1)}{k(t)}$$

The quantity k(t) is referred to as the effective multiplication constant; the total number of neutrons produced, on average, by one fast neutron from a previous fission event [23].

The point kinetics equations are [24]:

$$\frac{dn(t)}{dt} = \frac{(\rho(t)-\beta)}{\Lambda} n(t) + \sum_{i=1}^{Nd} \lambda i \, Ci(t) + S$$

$$\frac{dCi(t)}{dt} = \frac{\beta fi}{\Lambda} n(t) - \lambda i Ci(t) \quad i=1, 2, ..., Nd$$

Where t is the time (s), n is the neutron density (neutrons/m^3), C_i is the delayed neutron precursor concentration in group i (nuclei/m^3), β is the effective delayed neutron fraction ($\sum_{i=1}^{Nd} \beta i$), Λ is the prompt neutron generation time (s), ρ is the reactivity, f_i is the fraction

of delayed neutrons of group i ($\frac{\beta i}{\beta}$), β_i is the effective delayed neutron precursor yield of group i, λ_i is the decay constant of group i (s^{-1}), S is the source rate density (neutrons/m^3), and N_d is the number of delayed neutron precursor groups. These equations enable one to predict the time behavior of the neutron population in a reactor core induced by changes in reactivity.

3.2.2 Reactivity feedback

The reactivity in a reactor is a function of time, and of the neutron flux (or power level). Thus, a change in the power will be accompanied by temperature and density changes of the various reactor components that will impact reactor physics, resulting in a change of reactivity. These changes are called reactivity feedback effects. The concept of reactivity feedback is illustrated in Figure 3.7. There exist several reactivity feedback types, such as: coolant and moderator density or fuel temperature and density. The effects of fuel temperature and coolant/moderator density on reactivity will be further discussed in the sections 3.2.2.1 and 3.2.2.2.

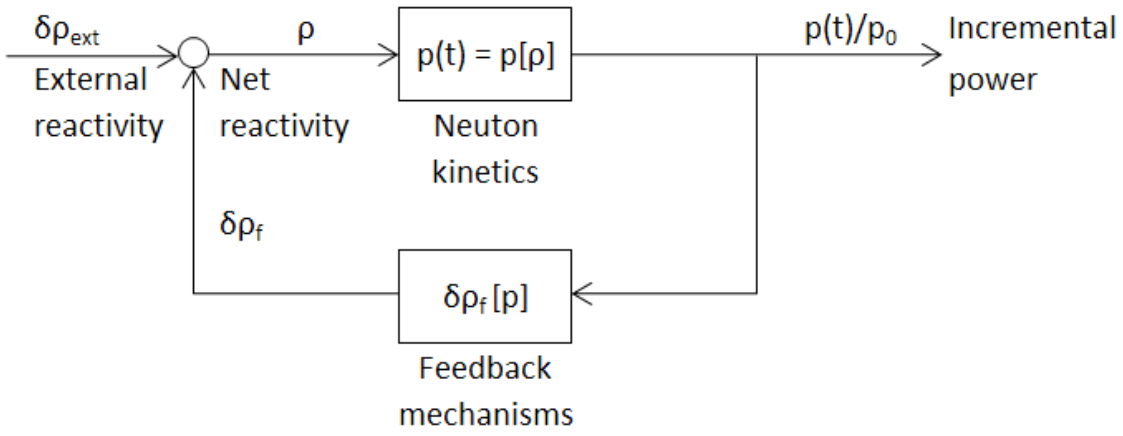

Figure 3.7: Closed loop block diagram [25]

3.2.2.1 Doppler temperature coefficient of reactivity:

The temperature coefficient of reactivity is defined as:

$$\alpha_T = \frac{\partial \rho}{\partial T} = \frac{\partial (k-1)}{\partial k} \sim \frac{1}{k}\frac{\partial k}{\partial T}.$$

With a view to increase safety, nuclear reactors are designed so that their Doppler temperature coefficient of reactivity is negative. Indeed, in that case, the reactivity of the core decreases with increasing temperature. For instance, if the power in the core increases, the fuel and coolant temperatures will increase. As a result of this temperature increase, the total reactivity of the system will decrease, and so will the power level. Similarly, a decrease in power will lead to an increase in reactivity. Negative feedback will tend to increase the reactor stability.

3.2.2.2 Coolant and moderator density effects:

As the temperature of the coolant or moderator increases, its density decreases. This change will impact the value of the reactivity. There are two moderators in the LS-VHTR reactor; the salt coolant and the graphite surrounding the coolant and the fuel. In this study, we will focus on the effects of coolant density changes on reactivity. These effects can be quantified with density feedback coefficient, defined as:

$$\rho_{dens} = \frac{\partial(\text{reactivity})}{\partial(\text{density})}.$$

3.2.3 Reactivity control

The reactivity of the core is affected by many factors, such as coolant density or fuel temperature as discussed in section 3.2.2. Thus, it is essential to control the total reactivity of the reactor at any time, in order to keep the reactor stable. The reactivity control of nuclear reactors is done by keeping the reactor critical ($\rho = 0$). A slight departure from criticality will self-stabilize due to a negative feedback. At operating conditions, reactivity control is achieved by using either: strong neutron absorbers in

solid shape called control rods, or absorbers dissolved in moderators that act as a poison (e.g. soluble Boron). For the start-up or shutdown of the reactor, control rods are used to change the reactivity of the core. During the start the reactor, the control rods are removed from the core at a certain rate to insert reactivity and make the reactor reach criticality. To shut the reactor down, control rods are inserted in the core to add negative reactivity and make the reactor subcritical (ρ negative).

3.3 Nuclear reactor shutdown process and decay heat

The nuclear plants are shut down for maintenance, refueling or in case of emergency. In the latter situation, the reactor is scrammed; all the control rods are instantly inserted in the reactor core, stopping the chain reaction. After a reactor scram, the power level decreases to some percentage of the steady-state value, because of the radioactive decay of fission products. The power generated by fission product decay is called decay power. Its initial value is about 6% of the steady-state power level if the reactor had held a constant power for a long period of time [26]. Then, decay power decreases exponentially with time, since no new fission products are created. Figure 3.8 shows the shape of the decay heat load after the shutdown of an AHTR-type reactor.

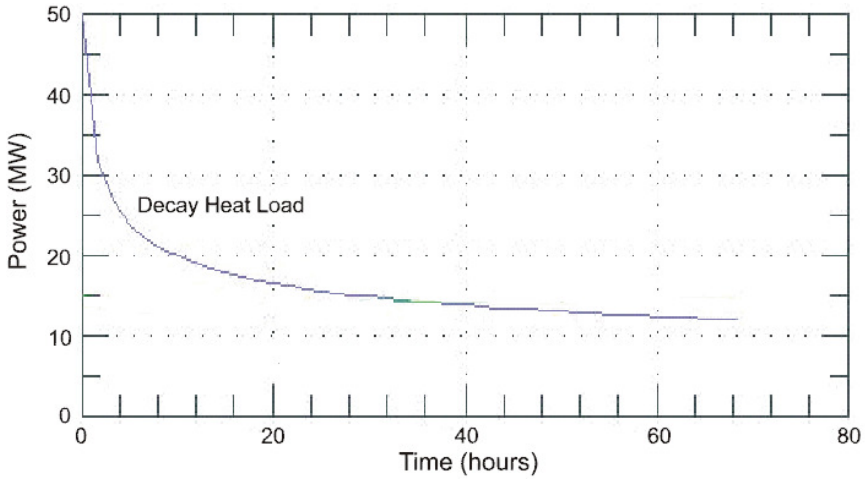

Figure 3.8: Decay heat load after the shutdown of the AHTR [2]

CHAPTER 4

METHODS AND MODELS

This section describes the development of the models and the methods used to develop, simulate and evaluate the passive start-up of a LS-VHTR.

4.1 Methods

To evaluate the start-up of the LS-VHTR with natural circulation of the coolant, the neutronics and thermal-hydraulic aspects of the reactor have been studied. The CSAS6 [27] package of SCALE6.0 [5] was used to perform neutronic calculations. The thermal-hydraulics and kinetics calculations and simulations were done by employing the RELAP5-3D [6] code. The methodology developed to simulate the start-up of the reactor was as follows.

A 3-dimensional model of one fuel assembly of the LS-VHTR core was developed with SCALE6.0. Several simulations were run with different fuel temperatures to calculate the temperature reactivity feedback of the fuel assembly. The density of the coolant was then varied from 1.80 g/cm^3 to 2.05 g/cm^3 to get the coolant density dependency of the fuel assembly. Given that the fuel temperature feedback and the coolant density feedback of the entire core of the reactor are expected to be similar, it was decided to make the simulations on the fuel assembly only, with proper boundary conditions.

In this study, we were essentially interested in understanding how the temperature, pressure, flow and power profiles would change during the start-up in the primary loop. Thus, only the primary loop and the intermediate loop of the nuclear power plant layout (see Figure 2.1) were modeled with the RELAP5 code. The primary loop, with FLiBe flowing through, was modeled as a closed loop in order to get as realistic

results as possible. Only the heat exchanger of the intermediate loop was accurately modeled, the inlet and the outlet of the heat exchanger were treated as boundary conditions. Fuel temperature and coolant density feedback from the neutronic calculations were entered in the RELAP5 model as an input. To get the initial conditions for the start-up simulation, two preliminary simulations were done. The reactor operation under steady-state conditions was first simulated. The shutdown of the reactor was then simulated using initial conditions from the previous simulation. Finally, using the reactivity feedbacks from the neutronics code, the thermal-hydraulic initial conditions from the shutdown simulation, and specifying a set of reactivity insertion steps (modeling the removal of the control rods) the start-up of the LS-VHTR plant was simulated. The results of these neutronics, kinetics and thermal-hydraulic simulations will be presented and analyzed later in this paper.

4.2 SCALE6.0 Model

The effort to analyze the reactivity changes with respect to fuel temperature and coolant density began by modeling the reactor fuel assembly in the Standardized Computer Analyses for Licensing Evaluation Modular Code System (SCALE6.0). The SCALE system was developed by ORNL and is capable of performing criticality, shielding, spent fuel depletion or decay, and reactor physics calculations [28]. All calculations were done using the Criticality Safety Analysis Sequence (CSAS6) with KENO-VI [29] package of the SCALE6.0 code. It was decided to use fresh fuel everywhere in the fuel assembly for simplicity. Also, all of the calculations were made at the beginning of life of the fuel, which is 10% enriched in U^{235}. Future work should reexamine these coefficients for different fuel burnups.

4.2.1 Materials

The three main materials encountered in the LS-VHTR core and modeled in SCALE6.0 are the fuel, the coolant, and the graphite used in the upper, lower and radial reflectors, and in the graphite blocks.

The TRISO fuel particles were modeled with the double-heterogeneity option of SCALE. The fuel kernel, carbon, and SiC layers composition were defined according to the specifications provided by ORNL and presented in Table 2.1. Because Silicon Carbide is a special mixture not recognized by the SCALE code, it was defined as a weight percent mixture of its isotopic components, with the natural isotopic abundance of Silicon (^{28}Si = 92.23%, ^{29}Si = 4.67%, and ^{30}Si = 3.1%). The TRISO particle volume fraction was set to 0.30 based on the range of values considered in literature.

The primary coolant composition, FLiBe (66% LiF, 34% BeF2), was also described as a weight percent mixture of its isotopic components. The FLiBe was assumed to be enriched to 99.99% ^{7}Li, given that it is difficult to produce Lithium with less than 0.01% of ^{6}Li [2].

It was decided to mix Boron with the graphite of the fuel assembly blocks and reflectors in order to get a multiplication factor around 1. Thus, a weight percent mixture of graphite and Boron 10 (99.9985% and 0.0015%) with a density of 1.74 g/cm^3 was defined for the material of the fuel assembly blocks and of the reflectors.

4.2.2 Fuel assembly

To accurately model the triangular pitch of the fuel assembly design, hexagonal lattice geometry was used to describe the fuel, coolant and graphite blocks. The fuel and coolant units are defined as a cylindrical form filled with fuel or FLiBe inserted in a hexagonal graphite block. These units were placed in an array to reproduce the pattern shown in Figure 2.4. A visual representation of the fuel assembly model is provided in Figure 4.1. The SCALE visualization tool GEEWIZ was used to generate the representation. Blue

units represent the fuel blocks, red units the coolant blocks, and the green units represent the graphite reflector blocks. The seven graphite blocks in the middle of the fuel assembly represent the fuel handling hole.

Mirror boundary conditions were set on the outer limit of the hexagon modeling the fuel assembly block. Thus, all the neutrons trying to escape the fuel assembly are reflected back, simulating the effect of adjacent fuel assemblies and axial graphite reflectors. This enabled us to make the calculations on the fuel assembly level and to assume that the results are similar to that we would obtain by simulating the whole core.

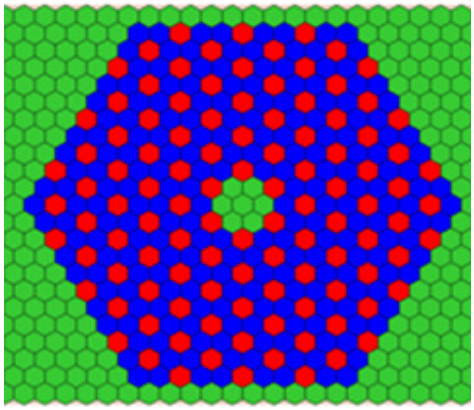

Figure 4.1: SCALE6.0 representation of the LS-VHTR fuel assembly

4.3 RELAP5-3D Model

Thermal-hydraulics analyses were performed using the Reactor Excursion and Leak Analysis Program (RELAP), developed at the Idaho National Laboratory (INL), which offers the capability to calculate the behavior of a reactor coolant system and the reactor kinetics during a transient. The RELAP5 code has been originally developed to model Light Water Reactors (LWRs). Though, the properties of several molten salts including FLiBe and FLiNaK have been subsequently incorporated [30], making the modeling of the LS-VHTR possible. The heat transfer coefficients used by RELAP5 for reactors with a salt coolant are the same as that used in the code to model LWRs, however, it was shown experimentally that this was an acceptable approximation.

4.3.1 Hydrodynamic components and main parameters

The model encompasses the core, the primary coolant (FLiBe) loop, two IHXs, and part of the intermediate coolant loop. The primary salt flows upwards through the core and downwards through the shell side of the IHX. The secondary coolant (FLiNaK) flows upwards through the tube side of the IHX. A schematic of the RELAP5 model is given in Figure 4.2. The components 10, 20 and 30 represent the coolant channels, corresponding to three core regions (inner, middle, outer). The core has been divided radially in three groups of fuel assemblies to increase the fidelity of the model (the method used to split the core will be presented in section 4.3.3). The core is divided in 8 segments axially. For example, for the component 10, segments 1 through 8 model the same fuel assemblies at different elevations.

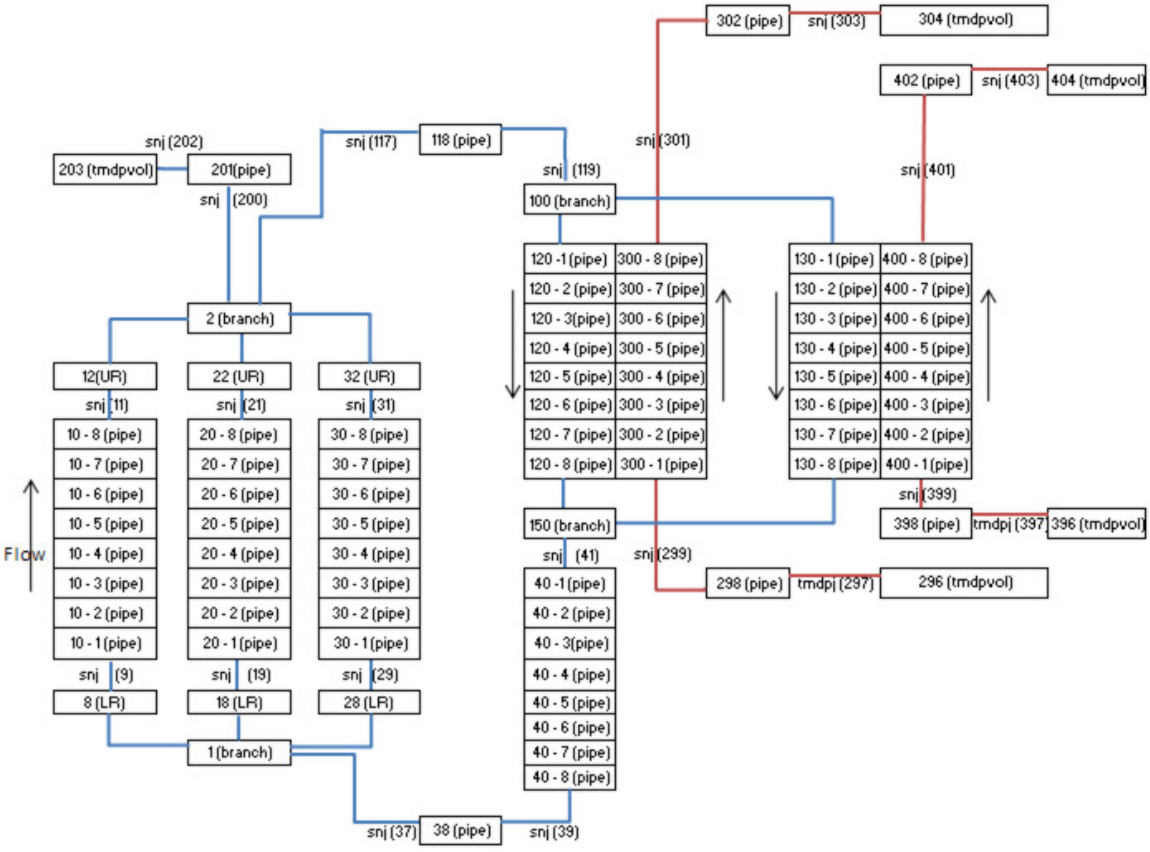

Figure 4.2: RELAP5 model of a LS-VHTR

The lower and upper reflectors are represented by the components 8, 18, 28 and 12, 22, 32 respectively. Given that the bypass flow in radial reflectors is assumed negligible (less than 5%), the radial reflectors were not modeled. Components 1 and 2 represent the lower and upper plenum respectively. The pipe 201 and the time dependant volume 203 model the pressure maintenance system above the upper plenum. The pipes 118 and 38 make the connection between the upper plenum and the upper header of the IHXs (component 100) at the top, and between the downcomer (component 40) and the lower plenum at the bottom. Components 100 and 150 represent the upper head and lower head of the IHXs. Components 120 and 130 represent the shell side of the IHXs, while components 300 and 400 represent the tube side of the IHXs. Components 296, 298, 302 and 304, 396, 398, 402 and 404 represent the secondary loop. Boundary conditions were specified in the junctions 297 and 397, in order to force the flow of the secondary loop.

The basic core design values are as follows in the RELAP5 model:

- Graphite block: 36 cm flat-to-flat, 8 m height
- Fuel cylinder modeling the fuel kernels of the TRISO particles: 0.6762 cm diameter
- Coolant channel: 0.953 cm diameter
- Core: 265 fuel assemblies
- Primary coolant: FLiBe ($2LiF\text{-}BeF_2$)
- Primary coolant expected steady-state temperatures: 1173 K inlet, 1273 K outlet
- Thermal power: 2400 MW
- Core flow: 10,000 kg/s

The dimensions and main parameters assumed for the other components are listed below:

- Top and bottom reflectors: 1m thick, same flow area as coolant channels

- Upper and lower plenums: 2 m and 1m height respectively, same flow area as the core
- Heat exchanger: shell and tube heat exchanger, see specifications in section 2.4
- Intermediate loop flow: 16,400 kg/s
- Intermediate loop steady state temperatures: 1140 K inlet, 1200 K outlet

The flow areas and length of the primary loop components were defined as follows:

- Plenum flow area: 2.032 m^2
- Inner assembly ring flow area and height: 0.284 m^2, 8 m
- Middle assembly ring flow area and height : 1.01 m^2, 8 m
- Outer assembly ring flow area and height : 0.736 m^2, 8 m
- Transport pipe flow area and length: 0.5 m^2 , 2 m
- Downcomer flow area and length: 0.5 m^2 , 3.2 m

The material properties (specific volumetric heat capacity and thermal conductivity) used in the analyses are as follows:

- Fuel: cp = 2.76e6 J/m^3K, k = 10.0 W/mK [7]
- Graphite blocks: cp = 3.276e6 J/m^3K, k = 30.0 W/mK [7]
- Coolant salt, FLiBe: cp= 4.39e6 J/m^3K, k = 1.1 W/mK [7]
- Hastelloy N alloy: cp = 5.12e6 J/m^3K, k= 23.6 W/mK [31]

4.3.2 Heat structures

Several heat structures have been defined in the model, attached to the coolant channels, the upper and lower reflectors, and the heat exchanger.

One heat structure has been implemented for each ring of the core (10, 20 and 30) to model the heat transferred to the coolant channels via the power generated by the fuel. The fuel heat structures are cylindrical, and their outer boundary is attached to the corresponding coolant channel hydrodynamic component. The RELAP5 code offers the

capability to model a simple fuel configuration only. For instance, the following type of fuel structure can be modeled in RELAP5: a cylindrical fuel rod surrounded by a cladding layer and an external layer of another material. The coolant channel is connected to the heat structure as a boundary condition. The fuel used in the LS-VHTR is a fuel compact, made of TRISO fuel particles assembled together in a graphite moderating matrix. Finding a model that would exactly reproduce the TRISO fuel performance was intricate. Thus, assumptions were made to model the fuel as accurately as possible. The fuel heat structure model is as follows:

- One cylindrical rod was defined to model the fuel
- A layer of graphite was set around the fuel to model the TRISO particle outer carbide layers, the graphite moderating matrix of the compact, and the graphite of the fuel assembly blocks

The radius of the rod modeling the fuel was calculated using the proportion of fuel in the TRISO particles (fuel kernel size) and the proportion of TRISO particles in the fuel compact (packing fraction). The calculated radius of the fuel rod is: $3.3771*10^{-3}$ cm. One should note that this may not be the most accurate way to model the performance of the TRISO particles with the RELAP5 code. Though, since this study aims at providing a model to evaluate the stability and feasibility of a start-up procedure with natural circulation, it was decided that this modeling of the fuel was the only practical option within the scope of this work, and adequate for the objectives. Further work would be needed to provide a more realistic model of the TRISO fuel, but this was out of the scope of this thesis.

Six heat structures have been defined to model the lower and upper reflectors. These heat structures are similar to the fuel heat structure, except that the material is graphite.

Each heat exchanger has an associated heat structure. The latter consists of a cylindrical layer of Hastelloy N alloy, with the secondary loop as the inner boundary

(tube side of the IHX) and the primary loop as the outer boundary (shell side of the IHX). The dimensions used for this heat structure were taken from Table 2.3 presented in section 2.4 of this study. For simplicity, it was decided not to model the baffles. The heat structure as presented models a simple straight-tube shell-and-tube type heat exchanger.

The heat losses in the plenums are assumed negligible. Thus, no additional heat structure has been defined.

4.3.3 Radial power distribution

The radial power distribution profile used was calculated by ORNL [10] and is shown in Figure 4.3. The distributions were generated using MCNP with a 10-ring core model. Given that the emphasis of this study is on the evaluation of the feasibility of a passive start-up, it was decided to split the core in only three regions (inner, middle, outer), which is deemed sufficient.

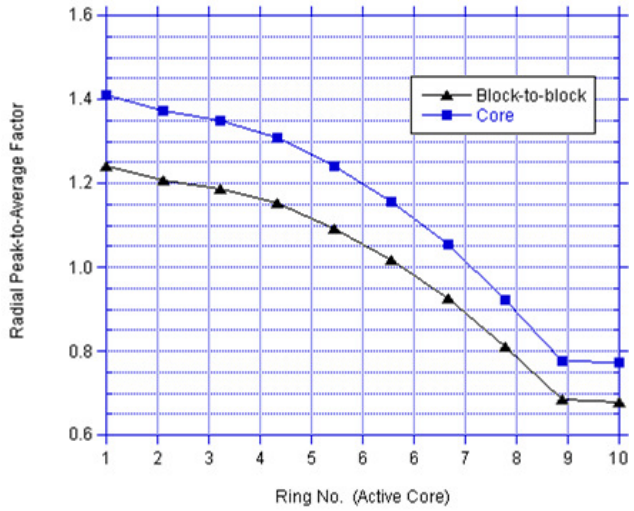

Figure 4.3: Radial power profile for the 10-ring ORNL LS-VHTR core [10]

An illustration of how the fuel assemblies were grouped to form three regions across the core is provided in Figure 4.4. The inner region groups the rings 1, 2, 3 and 4. The rings 5, 6, 7 and 8 constitute the middle region. The outer region is composed of the two outer rows of fuel assemblies; rings 9 and 10. A summary of the characteristics of

the groups is given in table 4.1. One can observe that the inner group produces more power per fuel assembly than the outer group.

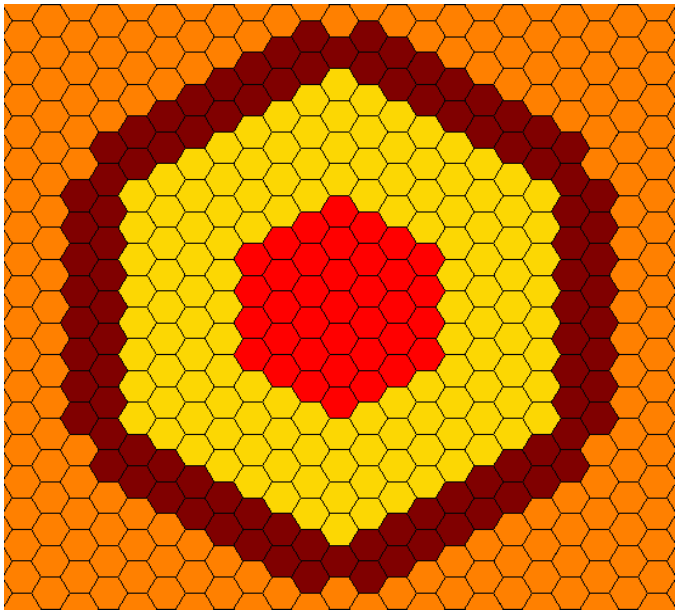

Figure 4.4: Inner, middle, and outer region of the LS-VHTR core

Table 4.1: Description of the model core regions

	Group 1 (inner)	Group 2 (middle)	Group 3 (outer)
Number of assemblies in the region	37	132	96
Fraction of total number of assemblies	14%	50%	36%
Power generated by the region	446.04 MW	1278.34 MW	673.80 MW
Fraction of total power	18.60%	53.30%	28.10%
Peak to average factor	1.33	1.07	0.78

4.3.4 Axial power distribution profile

The axial power distribution profile is used by RELAP to calculate the heat transferred to the coolant channels in each axial segment of the pipes modeling the core. An internal source multiplier value was specified for each axial segment of the three heat structures modeling the fuel channels of the three rings of the core. These values are multiplied by the total power (specified manually or calculated with the point reactor kinetics

equations) to obtain the power generated in the heat structure [32]. The axial power profile chosen is based on a profile used by ORNL to model the LS-VHTR [10]. This axial distribution was also used for gas-cooled VHTR modeling [33]. The power profile that was chosen is shown in Figure 4.5.

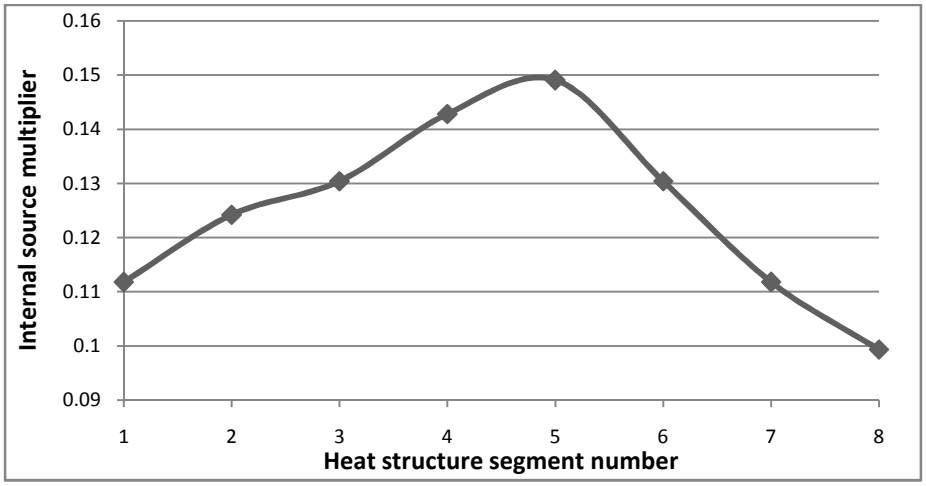

Figure 4.5: Typical Axial power distribution profile

To get the power profile in each region of the core, the distribution of Figure 4.5 was multiplied by the power generated in every region, as specified in table 4.1. The axial power distribution obtained for each group of fuel assemblies are shown in Figure 4.6.

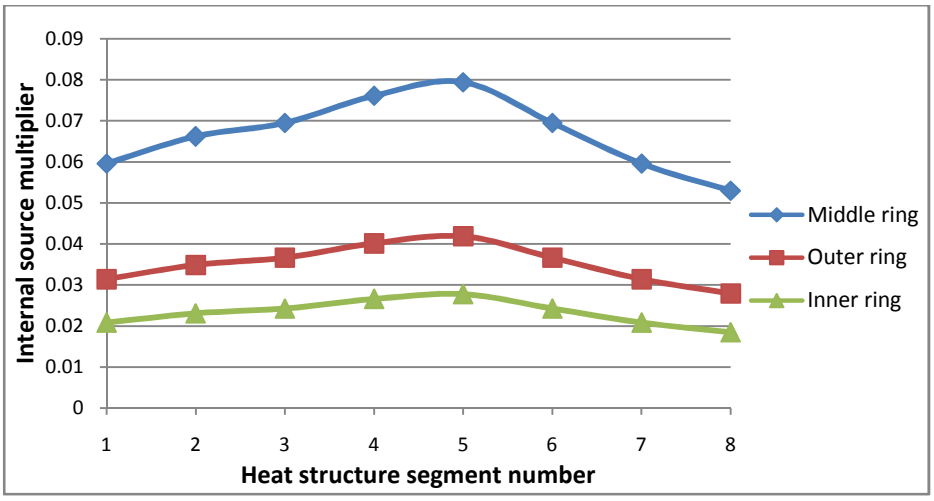

Figure 4.6: Axial power distribution profile in the core regions

4.3.5 Form loss coefficients

Given that the start-up of the LS-VHTR under natural circulation was studied, it was essential to take the flow resistance in the loop into account. To do so, form loss coefficients were specified to model the friction losses due to the abrupt area changes at the entrance of the lower axial reflectors and at the exit of the upper axial reflectors. Form loss coefficients were also specified at the entrance and the exit of the heat exchanger. Each loss coefficient was assumed to be 0.25, based on the typical loss coefficient used in LS-VHTR RELAP5 model [10]. In this study, the pump was not modeled with the RELAP5 component "pump". Instead, a time-dependant junction was used (junction 117 in Figure 4.2) to force the flow during steady-state conditions operation, and a simple junction was used to let RELAP5 calculate the flow during operation with natural circulation of the salt in the primary loop. A form loss coefficient of 1.0 was entered in the junction modeling the pump (in active or passive mode) to account for the pressure drop induced. This form loss coefficient was assumed. Thus, the behavior of the pump as modeled might differ from the behavior of the actual pump in the LS-VHTR design. This assumption impacts the value of the natural circulation mass flow rates predicted by the RELAP5 code and should be taken into account when observing the results of the different simulations that will be presented later in this report.

4.3.6 Reactor kinetics model

The point reactor kinetics model of RELAP5 offers the capability to compute the transient behavior of the neutron fission power in a nuclear reactor. It was used to calculate the reactivity changes and the power generated (by immediate fission of neutrons and by decay of fission products) during the start-up of the reactor. The RELAP5 code uses the point kinetics equations described in section 3.2.1 to calculate the power of the reactor. The decay power is calculated using the 1979 ANSI/ANS Standard

decay power model [34] [35]. The reactivity is calculated by RELAP5 as follows [6]:

$$r(t) = r_o - r_B + \sum_{i=1}^{n_s} r_{si}(t) + \sum_{i=1}^{n_c} V_{ci} + \sum_{i=1}^{n_\rho} \left[W_{\rho i} * R_\rho\left(\rho_i(t)\right) + a_{Wi} * T_{Wi}(t) \right] + \sum_{i=1}^{nF} \left[W_{fi} * R_F\left(T_{Fi}(t)\right) + a_{Fi} * T_{Fi}(t) \right],$$

where r_o represents the reactivity corresponding to assumed steady state power at t = 0, r_B is the bias reactivity calculated by RELAP5 such that $r(0) = r_o$, the quantities $r_{si}(t)$ represent the reactivity inserted at every time t, the quantities V_{ci} are control variables, R_ρ and R_F are tables defining reactivity as a function of the current moderator density $\rho_i(t)$ in the hydrodynamic volume i (density reactivity table) and reactivity as a function of fuel temperature in heat structure i (Doppler reactivity table), $W_{\rho i}$ is the density factor for volume i, $T_{Wi}(t)$ is the spatial density averaged moderator fluid temperature of volume i, a_{Wi} is the temperature coefficient for volume i, W_{Fi} and a_{Fi} are the fuel temperature weighting factor and the fuel temperature coefficient for heat structure i.

The values for the density reactivity table, Doppler reactivity table and for the temperature coefficient of reactivity were taken from the SCALE6.0 calculations. To model the reactivity insertion due to the removal of the control rods during the start-up of the reactor a table was entered defining the reactivity insertion curve as a function of time. Typical reactor physics values were used for the neutron delayed fraction and the prompt neutron generation time: $\beta = 0.0065$ (typical for U^{235}) [25], $\Lambda = 5*10^{-5}$ s [23].

A power history table was entered to make RELAP5 calculate the initial quantities of fission products, and thus the initial decay power for the reactor start-up simulation.

CHAPTER 5

RESULTS AND DISCUSSION

In this chapter the results of the LS-VHTR fuel assembly analysis done with SCALE6.0, and the RELAP5 simulations are presented. This chapter is organized as follows. Section 5.1 studies the effect of fuel temperature on the core reactivity, at constant coolant density. Section 5.2 performs the same examination but for changes in the salt coolant density. Section 5.3 presents the results of the steady-state simulation, and compares them to the steady-state conditions determined by ORNL in its conceptual design of the LS-VHTR. Section 5.4 examines the simulation of the reactor shutdown transient. Finally, section 5.5 presents the results of different single step reactivity insertion simulations, and analyzes a potential start-up procedure.

5.1 Doppler fuel temperature coefficient of reactivity

The simulations to calculate the Doppler coefficient of reactivity were done with CSAS6. When the CSAS6 code is run, cross sections are first generated. Then, the initial effective neutron multiplication factor (k_{eff}) of the system modeled is calculated by the program using the probabilistic KENO-VI Monte Carlo code. To get enough statistical precision on the multiplication factor, it was decided to run 1,000 generations with 10,000 neutrons per generation. This resulted in a 1σ statistical uncertainty ranging from $1.5*10^{-4}$ to $1.9*10^{-4}$.

The simulations were run with a coolant temperature of 1143K, which is the temperature of the coolant right before the reactor is started-up (this will be presented thoroughly in section 5.4). Seven simulations were run with fuel temperatures ranging from 873 K to 1473 K. The reactivity value (ρ) was calculated from the neutron multiplication factor value using the relation: $\rho = \frac{k_{eff}-1}{k_{eff}}$ (unit dk/k). The RELAP5 code

requires that the reactivity be entered in dollars ($) in the kinetics input. Thus, the value of the reactivity in dk/k unit was divided by the effective delayed neutron fraction ($\beta = 0.0065$) to convert it into $ unit. The results were arranged in a table and plotted. The equation of the relation between reactivity and fuel temperature ($\rho = \text{func}(T_F)$ were func is a function and T_F the fuel temperature) was extracted from this plot. The value of the derivative of this relation with respect to fuel temperature was finally calculated at different fuel temperatures to get the Doppler temperature coefficient of reactivity. The results of the CSAS6 simulations are presented in Table 5.1 and Figure 5.1 respectively.

Table 5.1: Doppler coefficient CSAS6 simulations results

T_F (K)	k_{eff}	ρ (dk/k)	ρ ($)	ρ(T) - ρ(873 K) ($)
873	1.0588	0.0555	8.5438	0.0000
973	1.0527	0.0501	7.7018	-0.8420
1073	1.04762	0.0455	6.9931	-1.5507
1173	1.04252	0.0408	6.2747	-2.2691
1273	1.03723	0.0359	5.5221	-3.0217
1373	1.03202	0.0310	4.7733	-3.7705
1473	1.02737	0.0266	4.0986	-4.4452

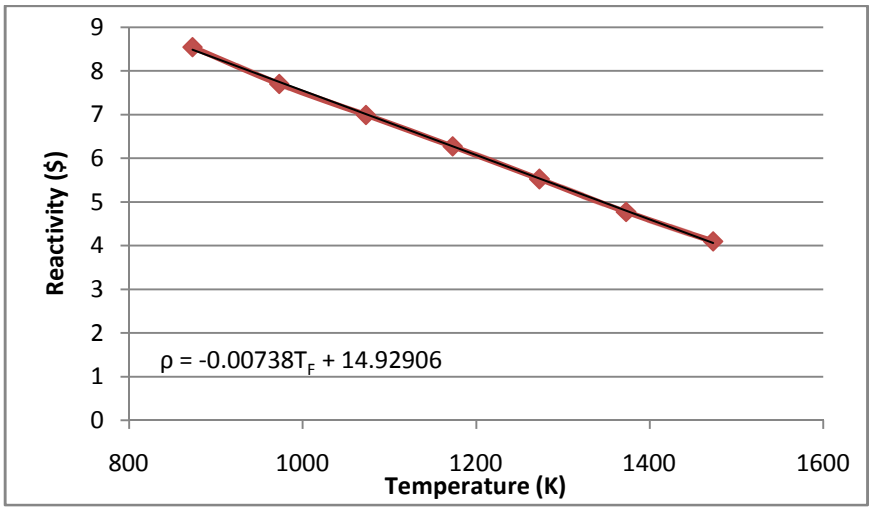

Figure 5.1: Calculated reactivity for 7 different fuel temperatures

The reactivity decreases with increasing temperatures. This means that the reactor has a negative Doppler fuel temperature coefficient, which was expected (see section 3.2.2.1).

The procedure to get the value of the fuel temperature coefficient is as follows. A linear fit was performed for the seven points and the equation of reactivity as a function of fuel temperature was obtained:

$\rho(T_F) = -0.00738*T_F + 14.821$ (\$)

The fuel temperature coefficient of reactivity is calculated by taking the derivative of this function with respect to fuel temperature:

$\frac{d\rho(TF)}{dTF} = -0.00738$ (\$/K).

Thus, the Doppler fuel temperature coefficient of the core is – \$0.00738 /K. This value is in acceptable agreement with the temperature coefficient estimated by ORNL for the AHTR: – \$0.01 /K [2].

5.2 Coolant density reactivity feedback

The simulations to evaluate the effect of changes of the coolant density were also done using CSAS6, with 1,000 generations per simulation, 10,000 neutrons per generation, and a 1σ statistical uncertainty ranging from $1.4*10^{-4}$ to $1.8*10^{-4}$.

The fuel temperature was set to 1150 K for all the simulations and the coolant temperature to 1140 K. These temperatures correspond to the average temperature in the fuel and coolant before the reactor is started-up. Simulations were run for six different FLiBe densities, ranging from 1.60 g/cm^3 to 2.15 g/cm^3. The same procedure as described in section 5.1 was then followed to calculate the reactivity of the system for the different densities. Results and plots of the simulations are given in Table 5.2 and Figure 5.2.

Table 5.2: Density coefficient CSAS6 simulations results

Coolant density (g/cm3)	k_{eff}	ρ (dk/k)	ρ ($)	ρ(dens) - ρ(1.80) ($)
1.60	1.0454	0.0434	6.6827	0.0000
1.65	1.0452	0.0432	6.6489	-0.0338
1.70	1.0447	0.0427	6.5756	-0.1071
1.75	1.0445	0.0426	6.5559	-0.1268
1.80	1.0441	0.0422	6.4924	-0.1903
1.85	1.0439	0.0421	6.4726	-0.2101
1.90	1.0437	0.0419	6.4402	-0.2425
1.95	1.0434	0.0416	6.3950	-0.2877
2.00	1.0430	0.0412	6.3384	-0.3443
2.05	1.0429	0.0411	6.3299	-0.3528
2.10	1.0425	0.0408	6.2719	-0.4108
2.15	1.0423	0.0406	6.2478	-0.4349

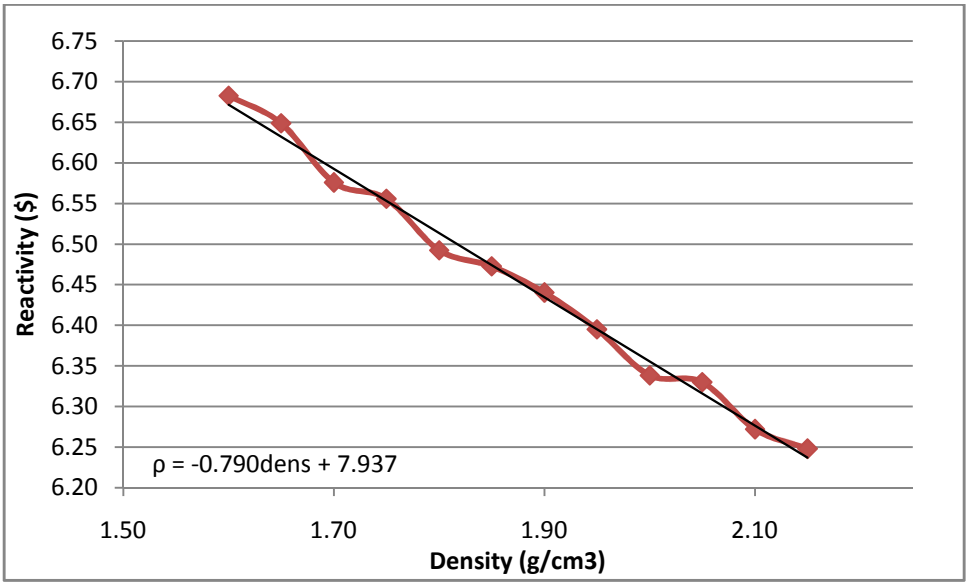

Figure 5.2: Calculated reactivity for 12 different coolant densities

The reactivity of the system decreases with increasing coolant densities. Given that an increase in coolant temperature results in a decrease of the coolant density, an increase in FLiBe temperature would lead to an increase of the reactivity of the system. This could lead to instabilities. Though, for a coolant density change of 0.25 g/cm^3, the

reactivity decreases from \$6.68 to \$6.47. The following correlation was used for the FLiBe density with respect to temperature [30]:

$\rho_{FLiBe} = A_D (T_{FLiBe} - 273.15) + B_D$

with A_D = -0.4884 kg/m^3/K, and B_D = 2279.7 kg/m^3.

It was calculated that densities ranging from 1.80 g/cm^3 to 2.05 g/cm^{3}correspond to temperatures ranging from 1250 K to 750 K. Thus, a coolant density decrease of 0.25 g/cm^3, corresponding to a coolant temperature increase of 500 K, would lead to about \$0.2 reactivity insertion. This effect is small, considering that during the start-up of the reactor, the temperature increase rate is usually on the order of magnitude of 50 K/hr. In addition, an increase in temperature also leads to a negative fuel temperature feedback that is much larger than the density feedback.

5.3 Steady-state conditions simulation and model verification

The aim of this simulation was to get the RELAP5 steady-state operating conditions of the LS-VHTR model. By steady-state operating conditions one means conditions at which the reactor operates after a long time of operation without variation in the power output or the coolant mass flow.

The simulation was run at a power level of 2400 MWth. The power was forced to this value by using a table of power versus time. The flow in the primary loop was forced to 10000 kg/s by using component 117 (see RELAP5 model nodalization in section 4.3.1) as a time dependant junction. Thus, the component 117 models the pump, driving the flow in the primary loop, just above the upper plenum. Initial conditions for this simulation were based on ORNL specifications for the LS-VHTR design [2], and are shown in Table 5.3. Two other time-dependant junctions were used to force the flow in the secondary loop to 16400 kg/s (8200 kg/s in each branch of the secondary loop). This simulation was arbitrarily run for 5000 seconds, given that it takes less than 1000 seconds for RELAP5 to converge to constant values of temperature and pressure.

Table 5.3: Initial conditions for the steady-state simulation

Thermal power (MW)	2400
Core outlet temperature (K)	1273
Core inlet temperature (K)	1173
Primary loop pressure (Pa)	2.30E+05
Primary loop flow (kg/s)	10000
Intermediate loop inlet temperature (K)	1133
Intermediate loop pressure (Pa)	2.30E+05
Intermediate loop flow (kg/s)	16400

The temperature and pressure profiles in the main components of the primary and intermediate loop given by the RELAP5 model at t up to 3500 s are presented in Figure 5.3, Figure 5.4, Figure 5.5, Figure 5.6, and Figure 5.7.

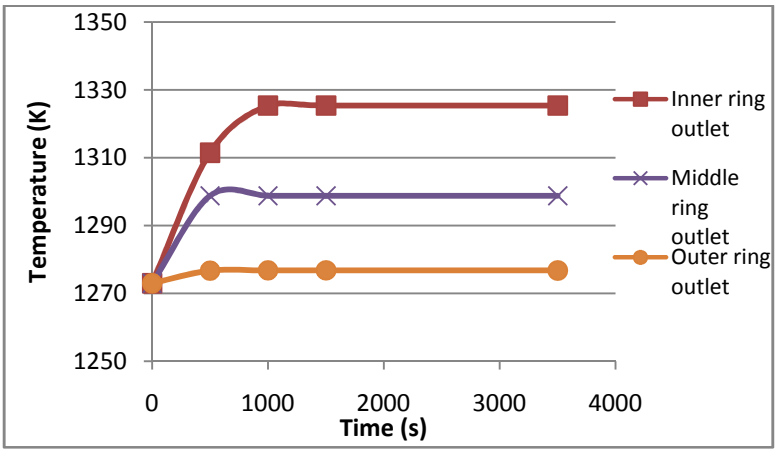

Figure 5.3: Coolant outlet temperatures in the three regions of the core

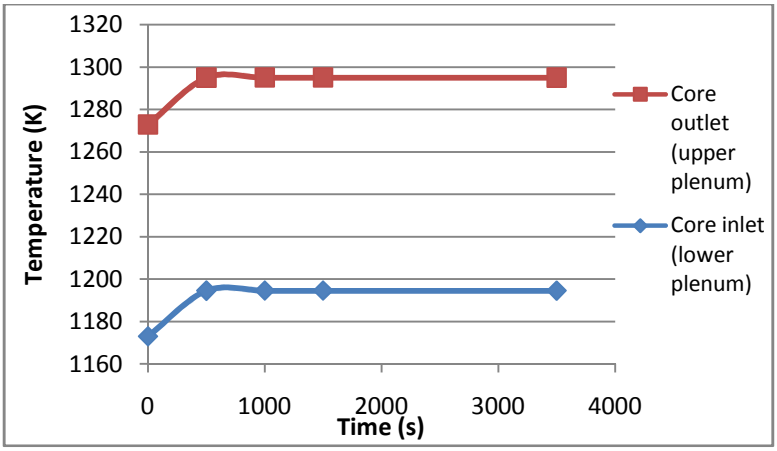

Figure 5.4: Core inlet and outlet temperatures

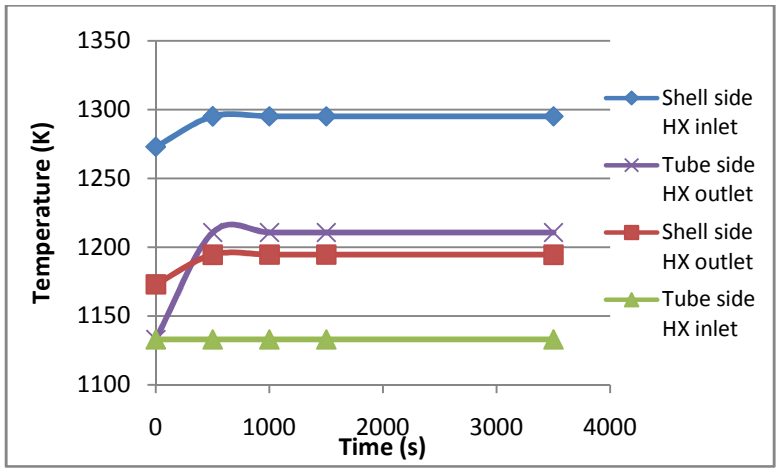

Figure 5.5: Inlet and outlet temperatures in the shell and tube sides of the heat exchanger

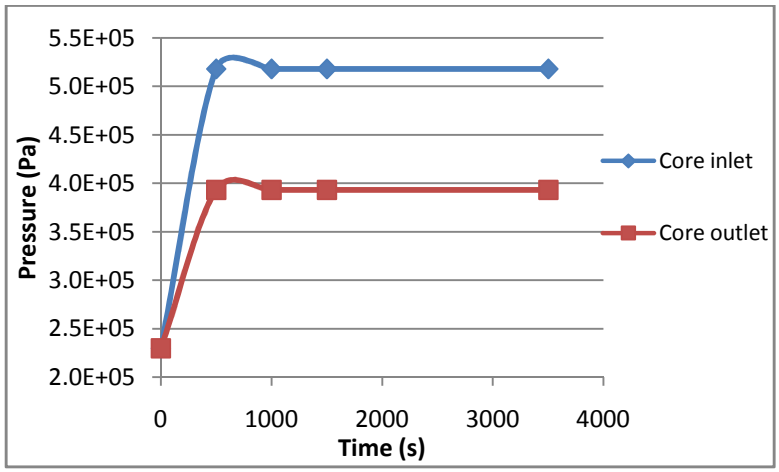

Figure 5.6: Pressure in the lower and upper plenums

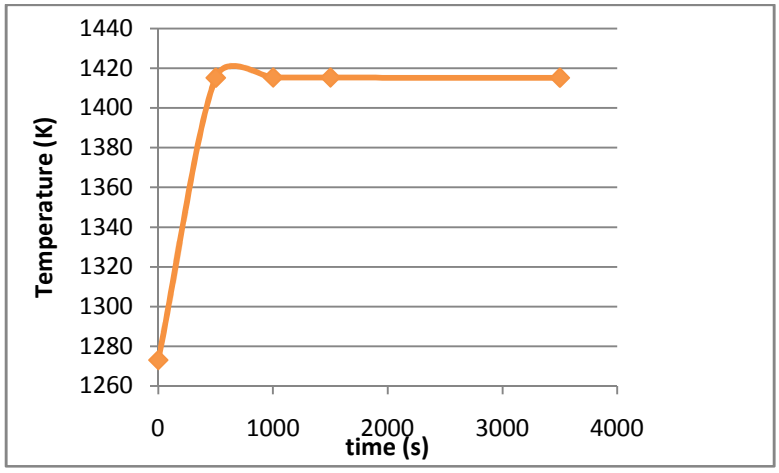

Figure 5.7: Peak fuel temperature of the core

After 1000 s, the values of temperature and pressure are steady. The temperature in the upper plenum is increased by 22 K, to reach at equilibrium 1295.0 K. The temperatures at the outlet of the three groups of fuel assemblies have changed so that the coolant outlet to inlet temperature difference across each ring is proportional to the amount of power they generate (see section 4.3.3). The temperature in the lower plenum increased to 1194.5 K. Thus, the RELAP5 steady-state temperature increase across the core is similar to what was initially specified. The temperature in the tube side of the IHX reached its equilibrium value, leading to a temperature drop across the heat exchanger in the secondary loop of 77.6 K. The peak fuel temperature calculated by RELAP5 is 1414.8 K., which is in acceptable agreement with the ORNL 2004 design peak fuel temperature [2]: 1433 K. Finally, the pressure in the primary loop has increased in the core and in the heat exchanger. We have not been able to fully explain this behavior, but believe that it does not significantly impact the subsequent analysis. ORNL specified in the 2004 report a core pressure drop of 0.129 MPa [2]. The core pressure drop of the RELAP5 model was calculated from the values in Figure 5.6 as 0.125 MPa. Thus, even if the pressure values of the RELAP5 model are higher than expected, the pressure drop across the core is coherent with the ORNL design.

The ORNL report also presents some values for the core inlet and outlet temperatures, and for the intermediate loop minimum and maximum temperatures [2]. A comparison between these values and the RELAP5 model developed in this study was established and is presented in Table 5.4.

Table 5.4: 2004 ORNL design and RELAP5 model primary and secondary loop temperatures

	2004 ORNL design	RELAP5 model
Core inlet temperature (K)	1173	1194.5
Core outlet temperature (K)	1273	1295.0
Core ΔT (K)	100	100.5
Inlet tube side HX temperature (K)	1133	1133.0
Outlet tube side HX temperature (K)	1193	1210.6
Tube side HX ΔT (K)	60	77.6

The core inlet and outlet temperatures of the RELAP5 model are 22.0 and 21.5 K higher than the corresponding values given by ORNL. The outlet temperature of the secondary loop is 17.6 K greater in the RELAP5 model. This difference may be due to the fact that the secondary side outlet temperature is higher in the RELAP5 model than in the ORNL design. It may also be explained by different specific heat capacities in the secondary side of the RELAP5 model and of the ORNL design, and by the fact that the heat exchanger used in this study was arbitrarily chosen. It was decided that this difference in temperature was acceptable given that this study focuses on the start-up and not on the operating temperature of the reactor.

5.4 Reactor shutdown simulation

This simulation is the continuation of the simulation presented in the previous section. Initial temperature, pressure and flow conditions of the shutdown simulation were taken from the steady-state simulation. The shutdown simulation with RELAP5 was done in order to get the temperature profiles and mass flows in the primary loop at certain time after the shutdown. Indeed, it simulates the thermal-hydraulic behavior of the reactor just after the loss of offsite power, when the reactor is scrammed.

To model the shutdown and the insertion of the control rods the power level is set at time 0.1 s to 139 MWth. The power decrease due to the absence of new fission events in the core is specified to RELAP5 using a power versus time table, and follows the ANS

standard decay power profile after shutdown [26]. The successive values entered for the power level are shown in Table 5.5.

Table 5.5: Power versus time table for shutdown simulation

Time (s)	Power (W)
0.0	2.40E+09
1.0	1.39E+08
5.0	1.32E+08
10.0	1.25E+08
50.0	9.60E+07
100.0	8.40E+07
500.0	6.00E+07
1000.0	5.28E+07
5000.0	3.60E+07
8000.0	3.00E+07
10000.0	2.88E+07
20000.0	2.40E+07
30000.0	2.04E+07

After the loss of offsite power, the circulation pumps of the primary loop coolant are switched off. To model this, the junction 117 was defined as a single junction, thus forcing the code to calculate the flow in the primary loop. The flow in the secondary loop was still forced to 16400 kg/s, assuming that batteries or diesel generators were used to keep the intermediate loop pumps running.

The LS-VHTR was designed with several safety features such as passive decay heat removal systems: the Reactor Vessel Auxiliary Cooling System (RVACS), the Direct Reactor Auxiliary Cooling System (DRACS), and the Pool Reactor Auxiliary Cooling System (PRACS). These systems offer the capability of passively (no external power needed) removing the decay heat from the core after a shutdown. In this study, we assume that there will be enough back-up power available to run the intermediate pumps. In case there would not be any power supplied by batteries or diesel generators, the reactor would be safely shut down using one of the passive decay heat removal systems listed above.

The reactor temperatures, mass flow and pressure changes over time calculated for the shutdown are shown in Figure 5.8, Figure 5.9, Figure 5.10, Figure 5.11, and Figure 5.12.

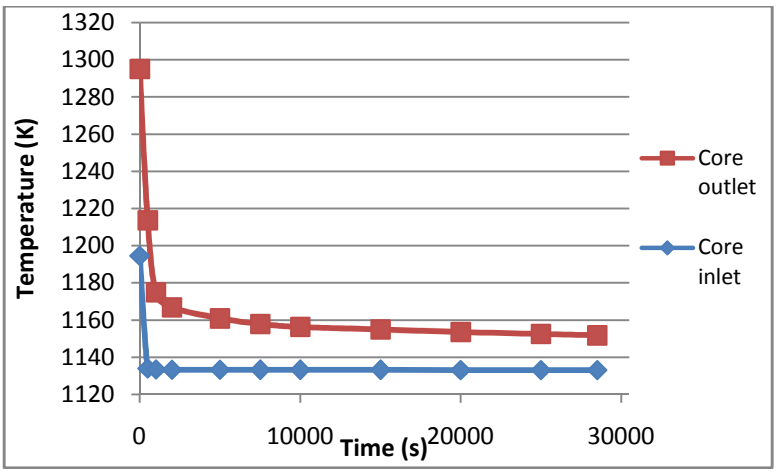

Figure 5.8: Inlet and outlet core temperatures

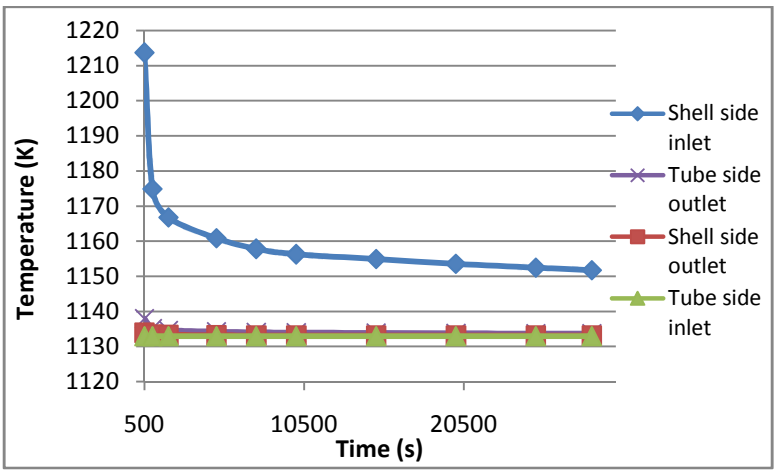

Figure 5.9: Inlet and outlet temperatures of the shell and tube sides of the IHX

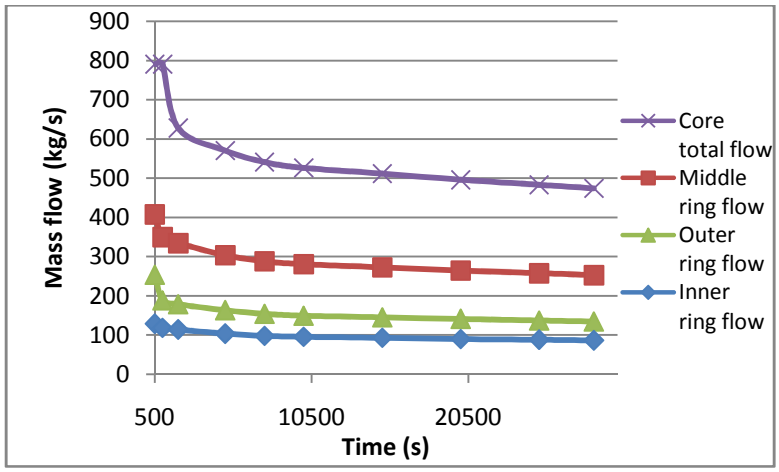

Figure 5.10: Mass flow in the core and in the different fuel assembly rings

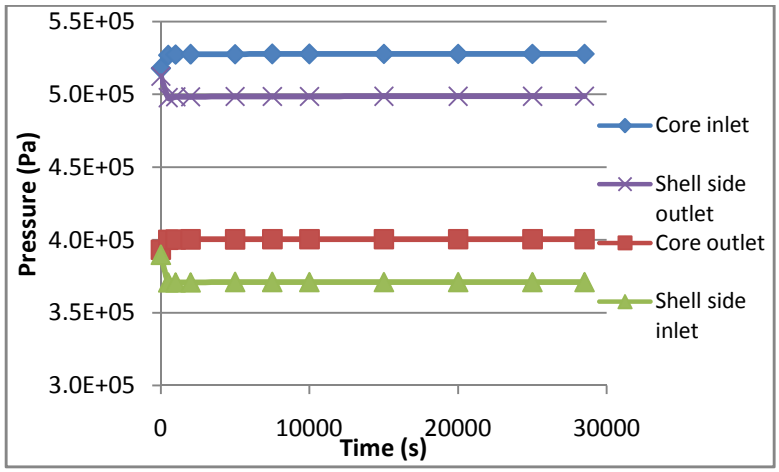

Figure 5.11: Pressure in the core and in the IHX

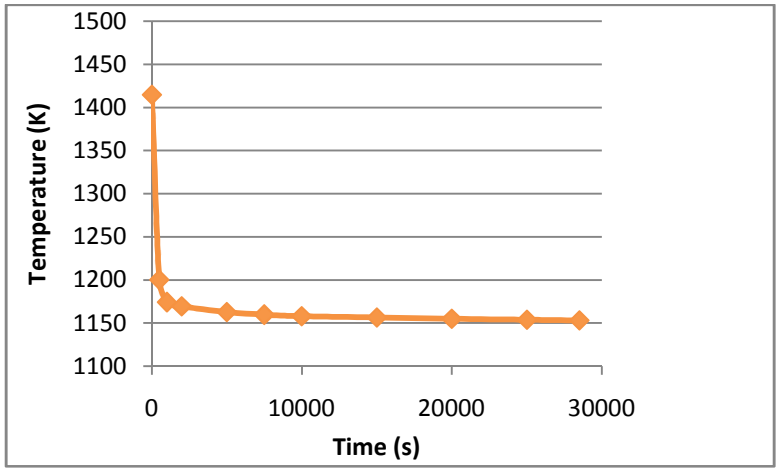

Figure 5.12: Peak fuel temperature in the core

One should note that in Figure 5.9 and 5.10, the first data point (time t = 0 s) has been omitted to optimize the display of the results (the initial mass flow and temperatures were too high compared to the next data point).

Table 5.6: RELAP5 model primary and secondary loop temperatures at the end of the shutdown period

	RELAP5 model
Core inlet temperature (K)	1133.11
Core outlet temperature (K)	1151.75
Core ΔT (K)	18.64
Inlet tube side HX temperature (K)	1133.01
Outlet tube side HX temperature (K)	1133.68
Tube side HX ΔT (K)	0.67

The temperature and flow decrease dramatically just after the scram of the reactor, like the power level. The core flow is equivalent to 7.9% of the steady-state core flow after 500 s and to 4.74% of the full condition flow after eight hours (28500 s). Between the time when the reactor is shut down and t = 500 s, the core inlet temperature is decreased by 60.6 K while the core outlet temperature drop is about 81.4 K. And between t = 500 s and t = 28500 s, the core inlet temperature did not significantly change while the core outlet temperature dropped by 61.9 K. Thus, there are significant changes for the first couple of minutes, and then the decrease in flow and temperature are much slower.

5.5 Reactor start-up simulations

To model the start-up of the reactor under natural circulation of the coolant, the kinetics mode of RELAP5 was used to calculate the power and reactivity changes of the core during the transient. The flow in the different rings of the core was also calculated by the program. The initial temperature, pressure and flow conditions are set to the final values obtained at the end of the shutdown simulation. The initial power consists of only decay

power (fission power is zero since the control rods are fully inserted), and is set to about 21.5 MW by specifying a power history table in the input file.

5.5.1 Results for step reactivity insertion simulations

Given the initial conditions determined in the previous simulations, several simulations were run to study the effect on the power level and thermal-hydraulic parameters of the core for different reactivity insertions, in order to determine limits on the amount of reactivity that could be inserted in the reactor core without jeopardizing its stability. While in reality the reactivity will most likely be inserted in a nearly-continuous fashion, in this analysis it was inserted stepwise, which is more challenging and may serve as a limiting representation of a fast control rod withdrawal. A table of reactivity versus time was used to model the reactivity insertion. Thus, there was no limit on the amount of reactivity to insert. In reality, the insertion of reactivity in the core is done by withdrawing the control rods from the core, and is thus limited to some amount, depending on the number, location, and worth of the control rods. It was assumed in this study that the total worth of the control rods in the core was sufficient to add up to \$1.55. The reactor response to single step reactivity additions was studied by running simulations with positive reactivity insertions ranging from \$0.1 to \$1.55. The results of these simulations are presented in the following paragraphs.

5.5.1.1 \$0.1 step reactivity insertion

In this simulation, \$0.1 of reactivity is inserted at t = 100 s. It was decided to wait 100 s before inserting the reactivity rather than doing it at time t = 0 s to allow the code to reach a steady state with the kinetics mode activated. Figure 5.13, Figure 5.14, Figure 5.15, and Figure 5.16 show the changes in reactivity, total power, decay, and fission power respectively during the transient that follows the insertion of reactivity in the core.

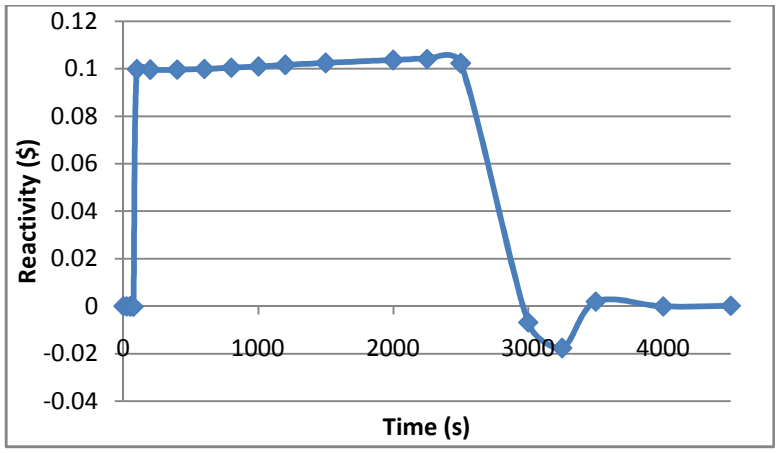

Figure 5.13: Core reactivity changes over time for $0.1 insertion

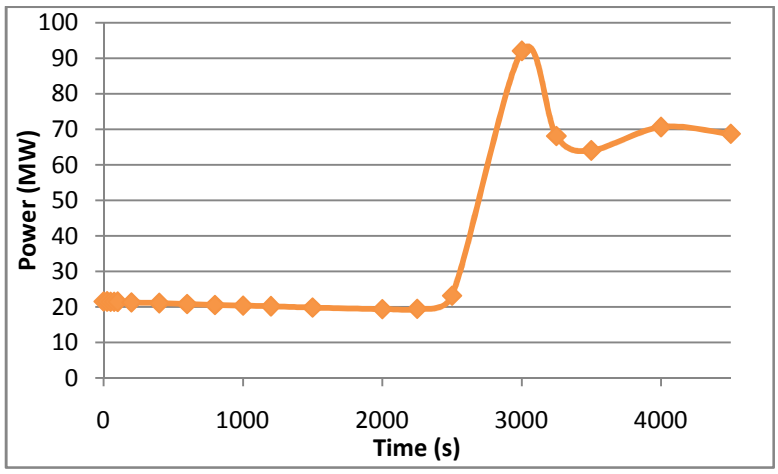

Figure 5.14: Total core power changes over time for $0.1 insertion

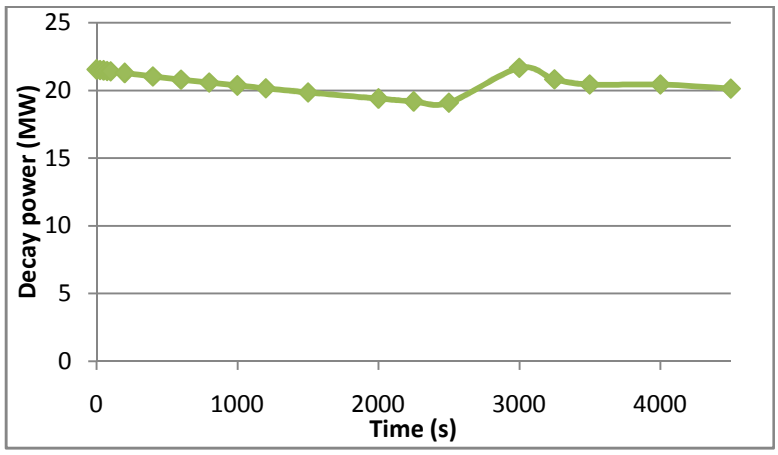

Figure 5.15: Decay power changes over time for $0.1 insertion

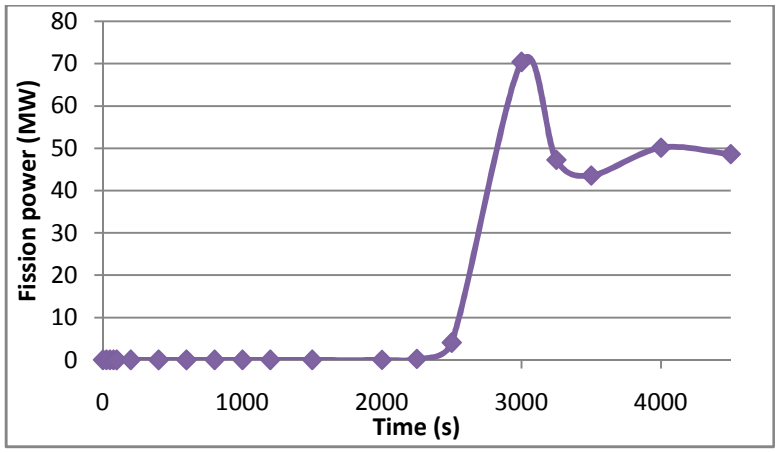

Figure 5.16: Fission power changes over time for $0.1 insertion

The positive reactivity is inserted at t =100 s, while the power swing occurs only after 2000 s. This can be explained by the prompt jump approximation [25]. In this approximation, the fission power is initially increased by the factor:

$$\frac{\beta}{\beta - \rho}$$

where ρ is the reactivity inserted. Then, the fission power increases exponentially by factor *e* in magnitude every reactor period. Given that the initial fission power equals $2.15*10^{-5}$ W, it takes a certain time for the fission power to increase to significant values even if the increase is exponential. That initial value of the fission power was calculated by RELAP5, based on the power history table that was entered, and thus may differ from the actual value of fission power in the LS-VHTR eight hours after a shutdown from full power condition. The total core reactivity goes to $0.1 after the insertion and remains at this value for about 2500 s. After this time, due to the feedback, the total core reactivity oscillates to stabilize again at its initial $0 value at t = 3500 s. Thus, it takes about an hour for the core to stabilize after a $0.1 positive reactivity insertion. The decay power slowly decreases until 2500 s, since no significant new fission occurs, and then increases because of the new fissions happening in the core. The results plotted show that the power level is increased from 21.5 MW to 68.76 MW.

The core inlet and outlet temperature, the total core mass flow and the fuel centerline peak temperature in the inner ring are shown in Figure 5.17, Figure 5.18, and Figure 5.19.

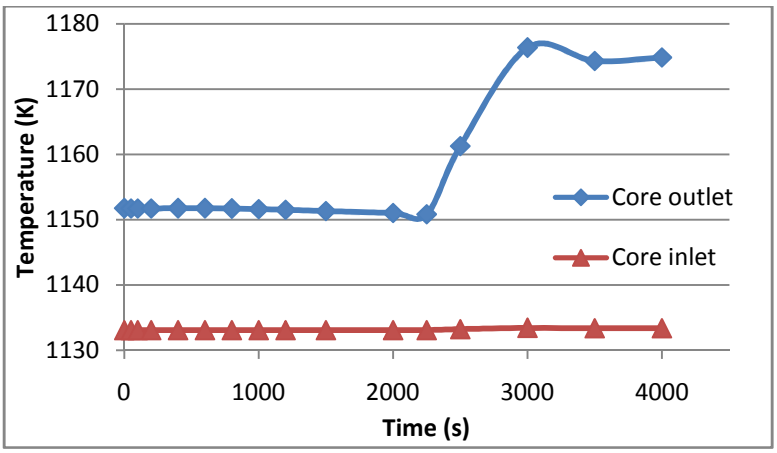

Figure 5.17: Core inlet and outlet temperature changes over time for $0.1 insertion

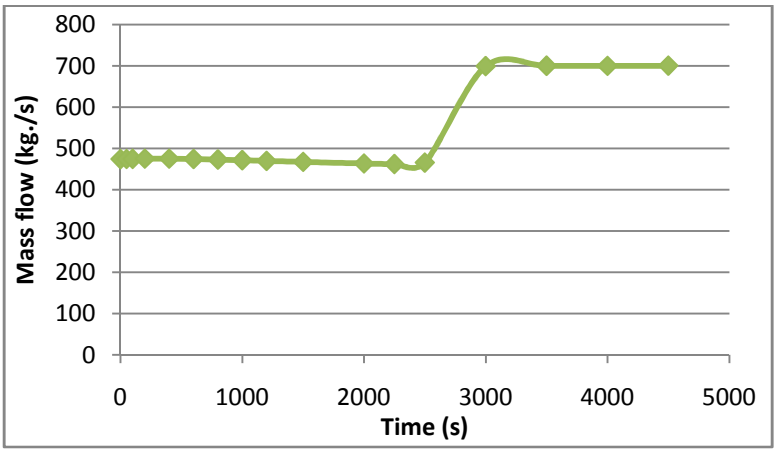

Figure 5.18: Total core mass flow changes over time for $0.1 insertion

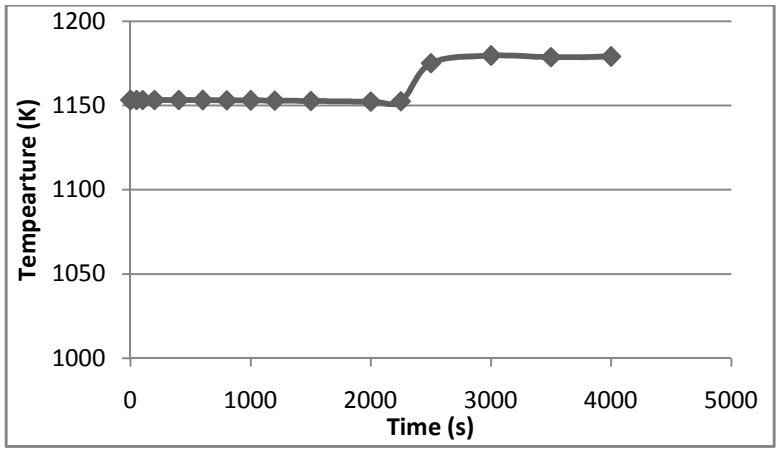

Figure 5.19: Fuel centerline peak temperature in the inner ring changes over time for $0.1 insertion

The core outlet temperature and the peak fuel centerline temperature reached 1174.9 and 1179 K. The small temperature differential is due to the fact that even if the power is increased by more than a factor of 3, it is still only a small fraction of the full power of the reactor. It should be noted that the fuel temperature calculated by RELAP5 during the start-up may slightly differ from the actual fuel centerline temperature in the LS-VHTR. This is due to the fact that the TRISO fuel was modeled as a cylindrical fuel element surrounded by graphite, as explained in section 4.3.2. This is an approximation that may impact the calculations of the fuel temperature. The total core mass flow was increased by 226.1 kg/s and its final value is 700.3 kg/s. This final value for the total mass flow rate should be observed with caution. Indeed, even if the RELAP5 code evaluation of the natural circulation mass flow rate is expected to be accurate [36] [37], the form loss coefficients entered in the model to account for the friction losses in the loop were chosen based on literature values and engineering judgment, and did not result from detailed evaluation of the specific design. Thus, the calculations made by the RELAP5 code in these simulations provide only an approximation of the mass flow rate that may be achieved with natural circulation.

5.5.1.2 $0.15 step reactivity insertion

The effect of adding $0.15 reactivity at t = 100 s was then evaluated. The procedure is similar to that for the $0.1 insertion simulation. Figure 5.20, Figure 5.21, Figure 5.22 and Figure 5.23 show the changes in reactivity, total power, decay, and fission power respectively during the transient that follows the addition of reactivity to the core.

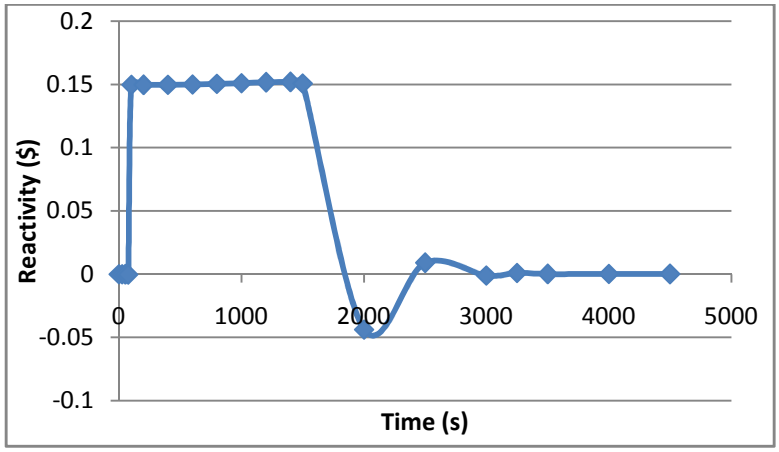

Figure 5.20: Core reactivity changes over time for $0.15 insertion

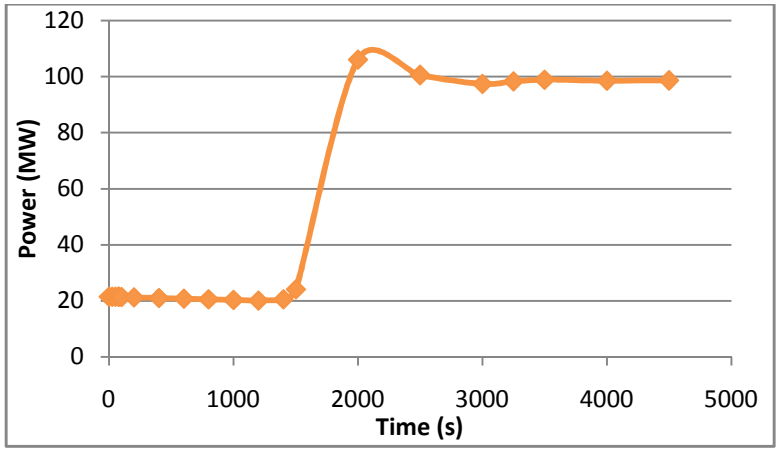

Figure 5.21: Total core power changes over time for $0.15 insertion

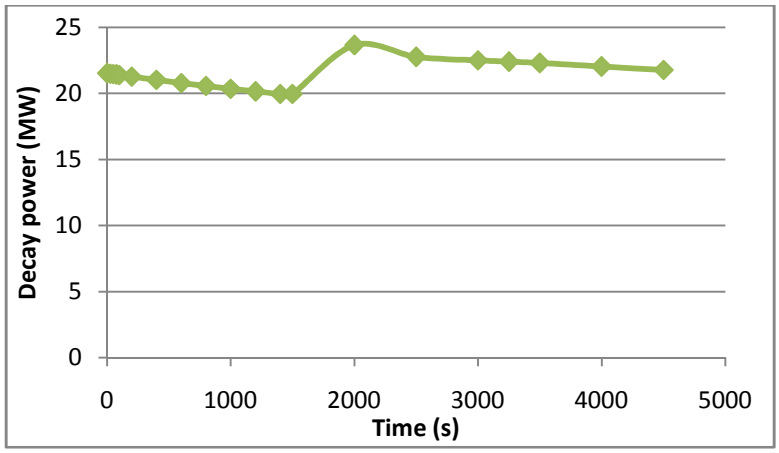

Figure 5.22: Decay power changes over time for $0.15 insertion

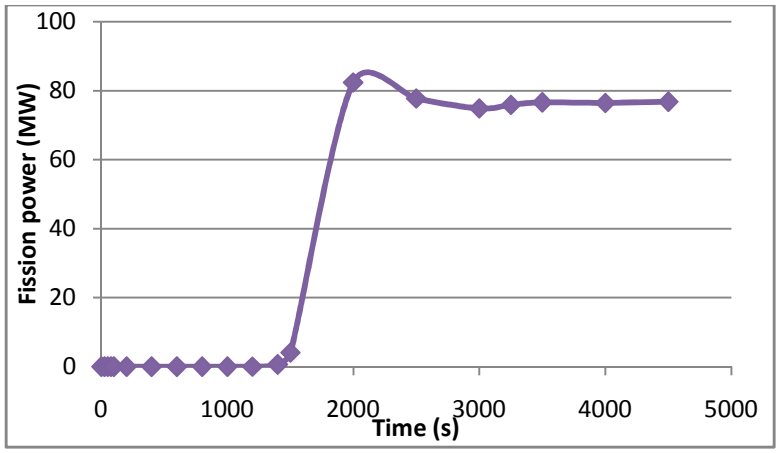

Figure 5.23: Fission power changes over time for $0.15 insertion

The core inlet and outlet temperature, the total core mass flow and the fuel centerline peak temperature in the inner ring of fuel assemblies are shown in Figure 5.24, Figure 5.25, and Figure 5.26 respectively.

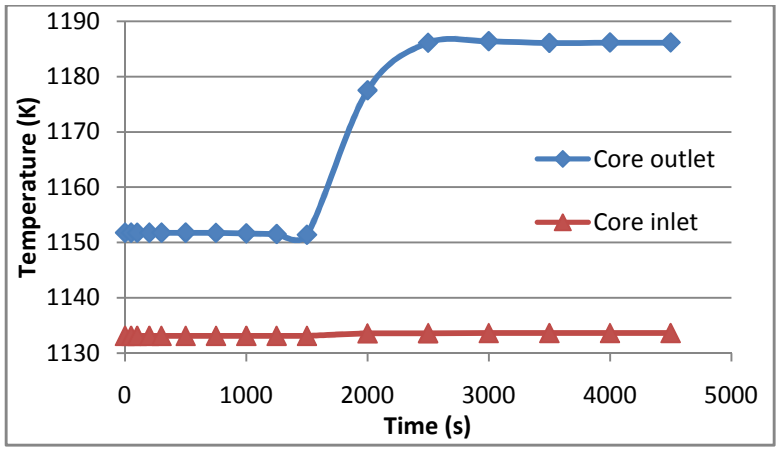

Figure 5.24: Core inlet and outlet temperature changes over time for $0.15 insertion

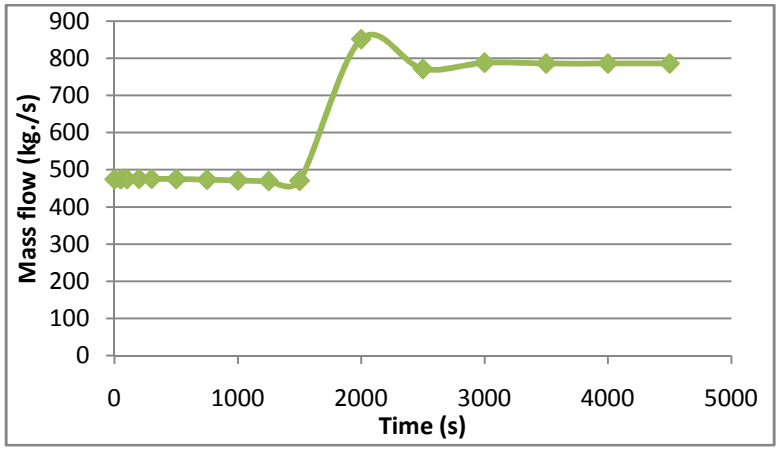

Figure 5.25: Total core mass flow changes over time for $0.15 insertion

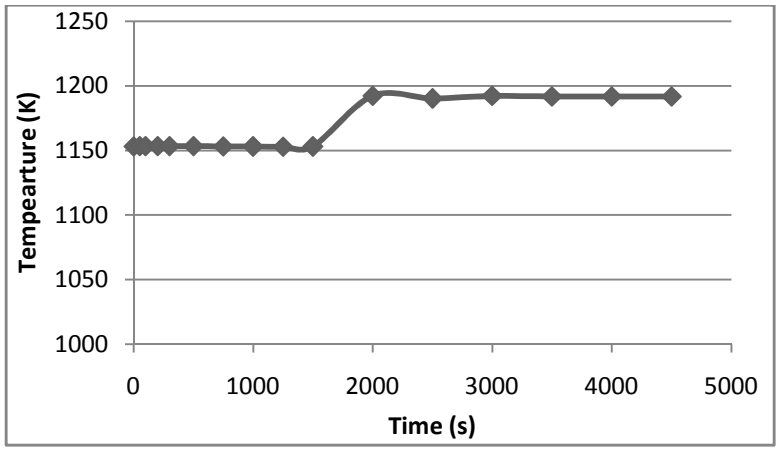

Figure 5.26: Fuel centerline peak temperature in the inner ring changes over time for $0.15 insertion

The response of the system to a \$0.15 addition is similar to that for a \$0.1 insertion, with a different magnitude, and an increase of fission power is observed sooner (around 1500s). The power is increased from 21.5 MW to 98.5 MW. The core inlet, outlet, and fuel centerline peak temperature are at the time t = 4500 s: 1133.6, 1186.1 and 1191.8 K. The mass flow driven by natural convection is increased from 474.2 kg/s initially to 785.7 kg/s at the end of the simulation.

In order to provide a thorough understanding of the phenomena happening during the transient following the control rods removal, other thermal-hydraulic parameter values are plotted in Figure 5.27 to Figure 5.29. These figures show the mass flow and temperature changes in the three regions of the core during the transient.

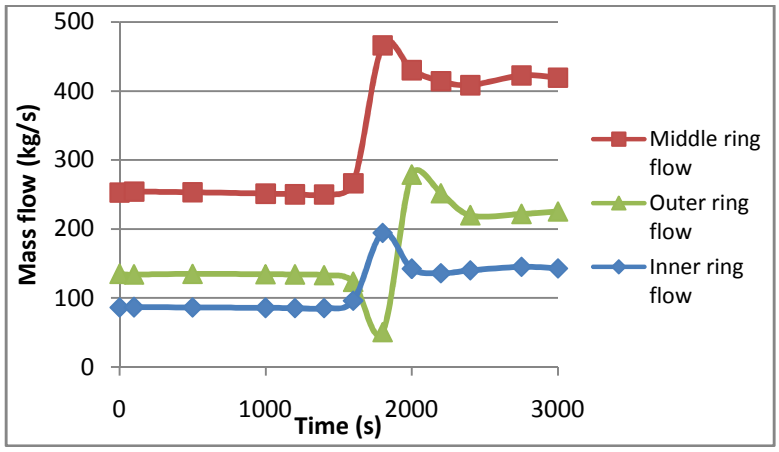

Figure 5.27: Flow in the different rings of the core for \$0.15 insertion

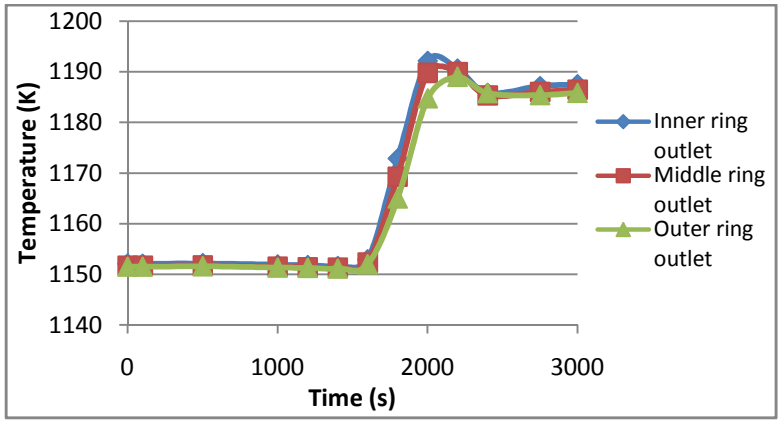

Figure 5.28: Coolant outlet temperature in the different rings of the core for \$0.15 insertion

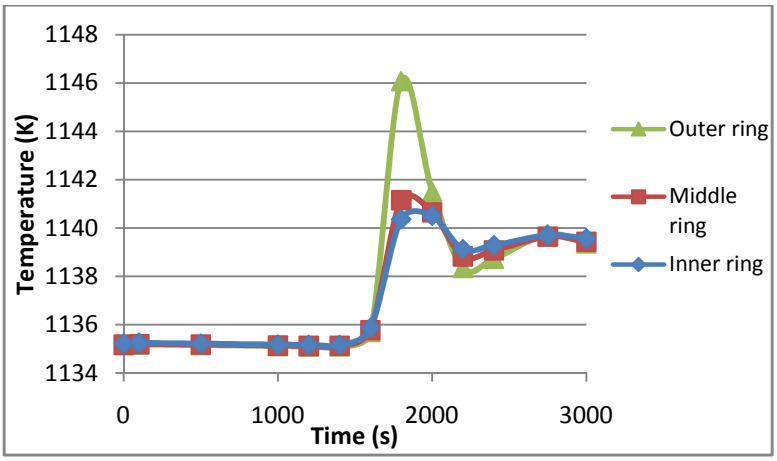

Figure 5.29: Coolant temperature of the first axial segment in the different rings of the core for $0.15 insertion

The effect of the reactivity insertion on the flow and temperatures in the inner, middle and outer rings of the core can be seen after 1500 s. Due to the significant power increase, the outlet and inlet temperatures are increased. The outlet temperature increase equals about 38 K in the three core regions. Though, the temperature increase in the first axial segment of the inner region is twice as high as the increase in the inner or middle assemblies. This leads to a lower temperature differential in the outer region of the core than in the inner and middle region. As a consequence of the varying temperature increases, the coolant behaves differently in each region of the core. Figure 5.27 shows that from t = 1200 s to t = 1800 s the mass flow in the outer fuel assembly ring decreases. This decrease is due to the natural circulation of the coolant, and should be kept limited to avoid counter-flow.

5.5.1.3 $0.5 step reactivity insertion

In this section, the effect of a $0.5 reactivity insertion was examined. The results of this simulation are presented in Figure 5.30 to Figure 5.36.

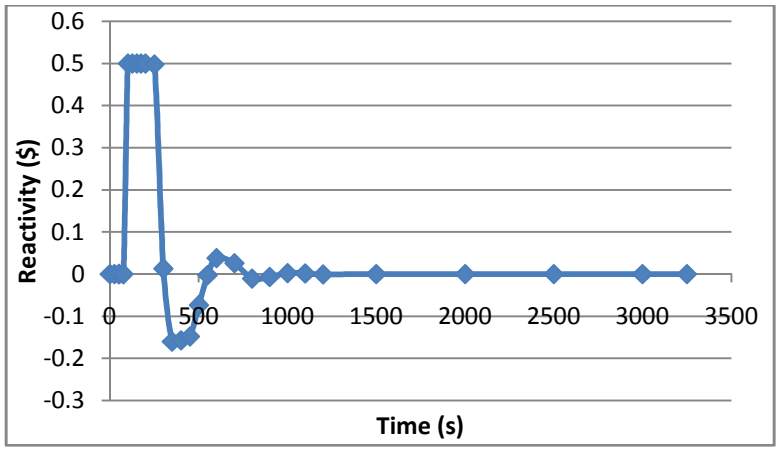

Figure 5.30: Core reactivity changes over time for $0.5 insertion

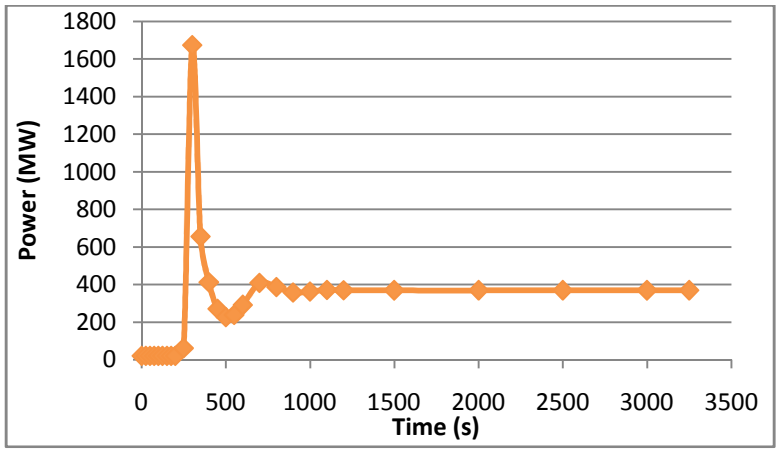

Figure 5.31: Total core power changes over time for $0.5 insertion

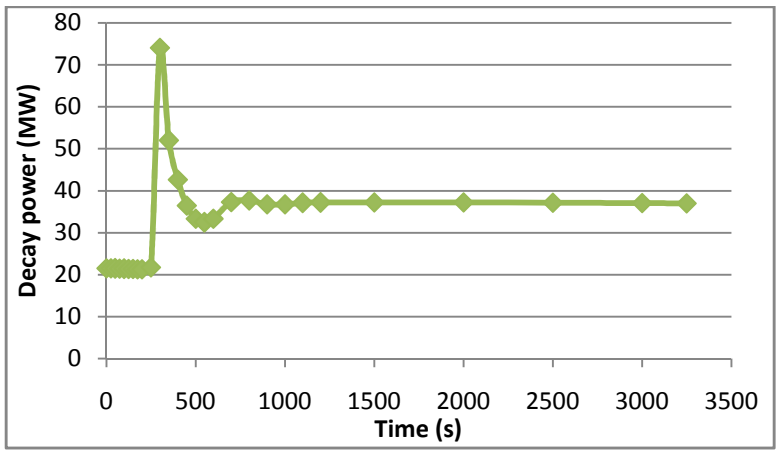

Figure 5.32: Decay power changes over time for $0.5 insertion

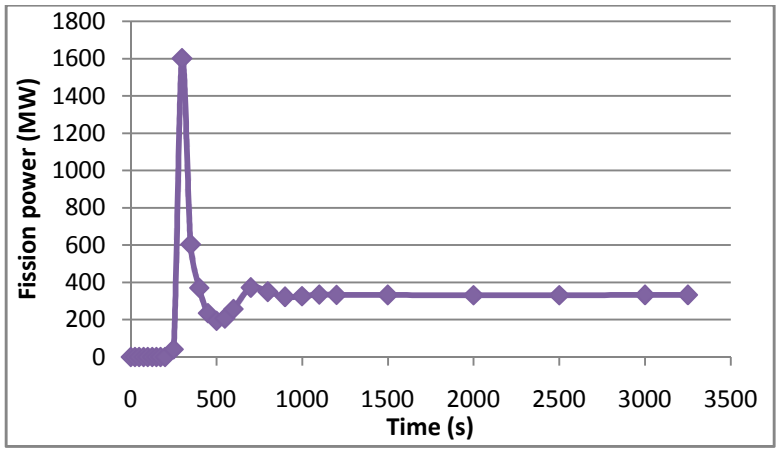

Figure 5.33: Fission power changes over time for $0.5 insertion

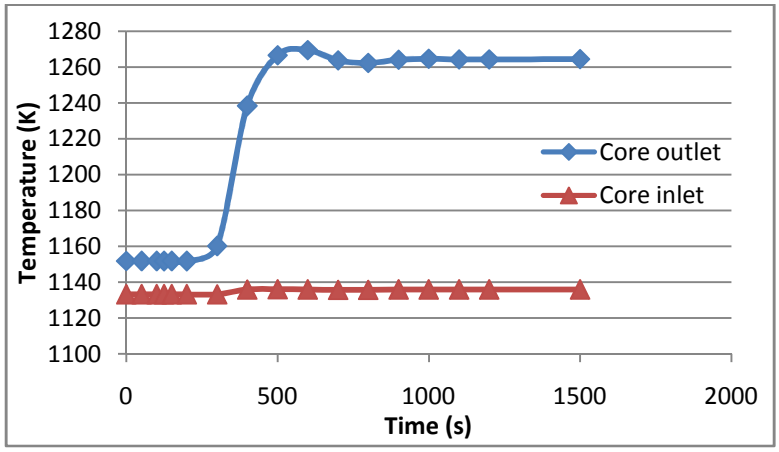

Figure 5.34: Core inlet and outlet temperature changes over time for $0.5 insertion

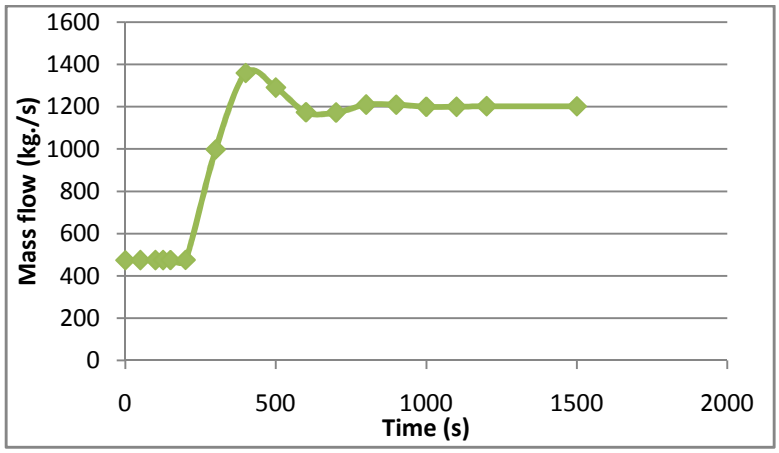

Figure 5.35: Total core mass flow changes over time for $0.5 insertion

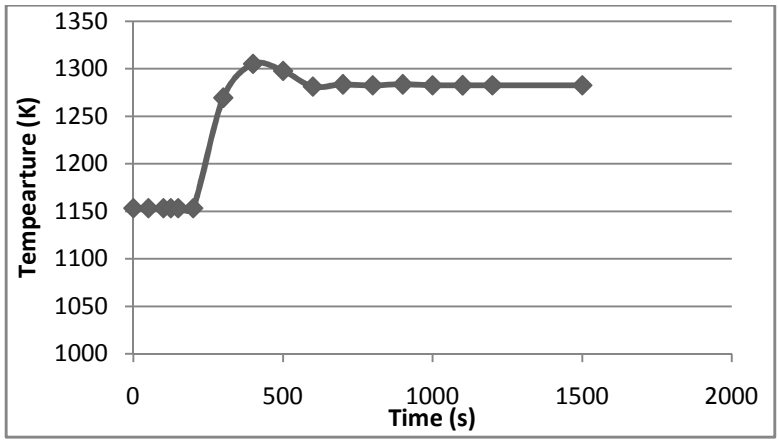

Figure 5.36: Fuel centerline peak temperature in the inner ring changes over time for $0.5 insertion

The addition of $0.5 reactivity to the core led to equilibrium values of power, flow and temperature as follows. The power level and total core flow reached 369 MW and 1201.6 kg/s at t = 1000 s. The core outlet and fuel centerline temperatures are increased to 1264.3 and 1282.7 K respectively. Moreover, the total core reactivity response time to the positive insertion is shorter than that for a $0.15 insertion. Indeed, after the insertion, the reactivity value remains constant for 250 s, and then oscillates until it reaches an equilibrium value after 1200 s.

5.5.1.4 $1.0 step reactivity insertion

The results of a $1.0 step reactivity insertion are shown in Figure 5.37 to Figure 5.43.

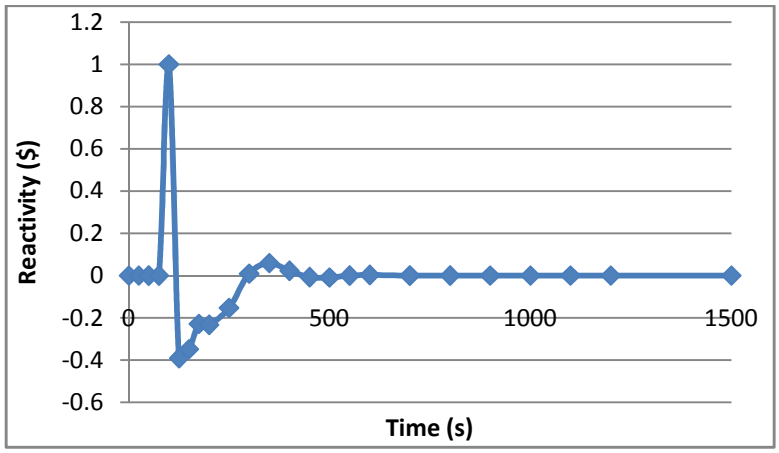

Figure 5.37: Core reactivity changes over time for $1.0 insertion

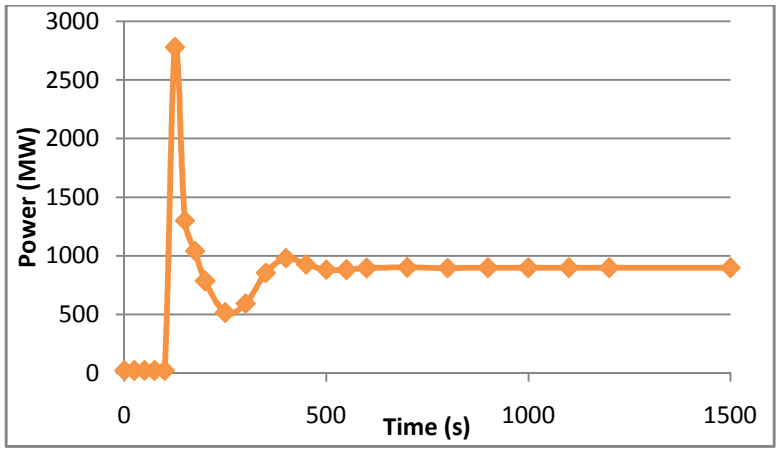

Figure 5.38: Total core power changes over time for $1.0 insertion

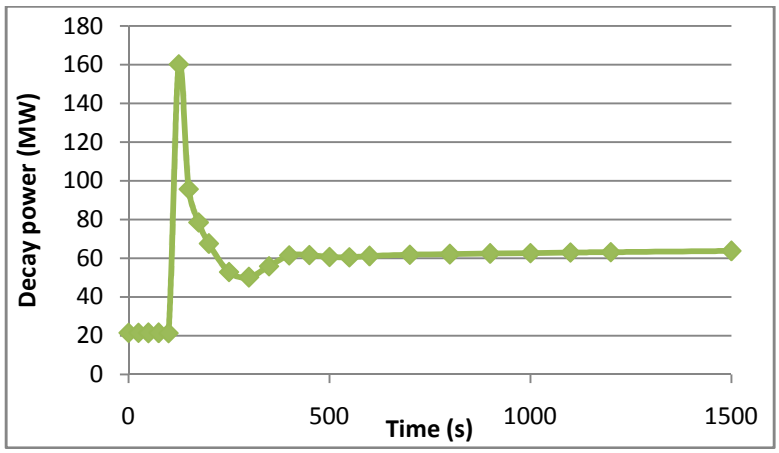

Figure 5.39: Total decay power changes over time for $1.0 insertion

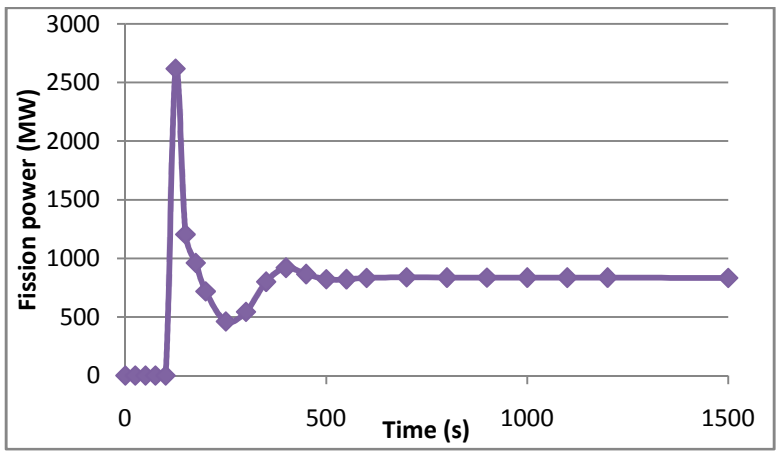

Figure 5.40: Total fission power changes over time for $1.0 insertion

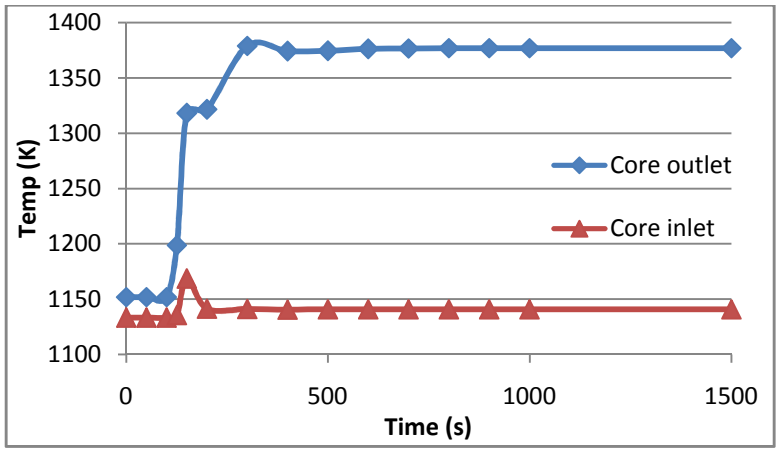

Figure 5.41: Core inlet and outlet temperature changes over time for $1.0 insertion

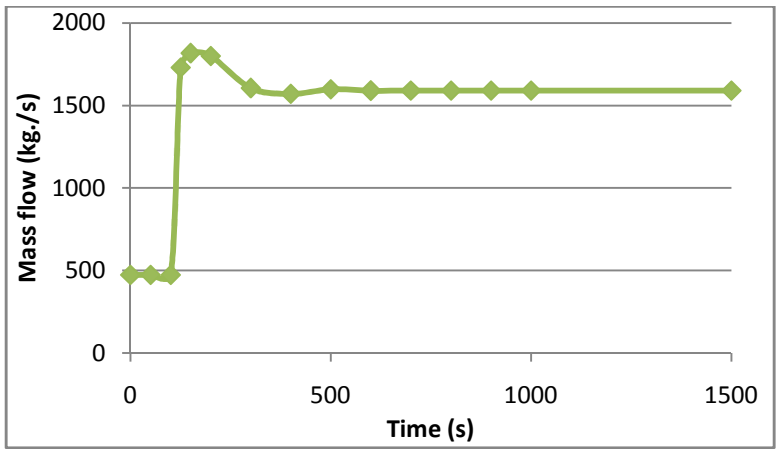

Figure 5.42: Total core mass flow changes over time for $1.0 insertion

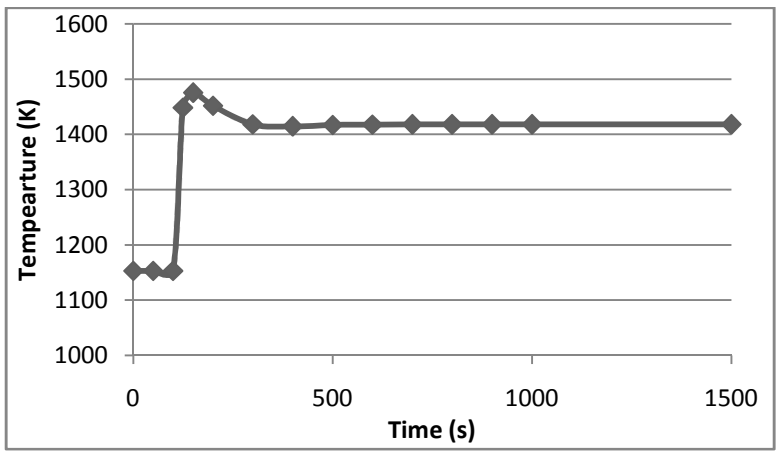

Figure 5.43: Fuel centerline peak temperature in the inner ring changes over time for $1.0 insertion

The temperature, flow and power profiles for $1.0 reactivity insertion are similar to that for $0.5 insertion. The reactivity jumps to $1.0 at t = 100 s, and then oscillates to reach its equilibrium value at t = 900 s. The reactor response time is faster but the time to stabilize is increased in comparison with the time for the reactor to respond to a $0.5 reactivity insertion. The power level and total core flow reach 897 MW and 1590.9 kg/s. The core outlet and fuel centerline temperatures are increased to 1377 and 1418 K respectively.

Other thermal-hydraulic parameter changes over time are presented in Figure 5.44 to Figure 5.46 in order to show the behavior of the coolant in the three rings of the core during the transient following the reactivity swing.

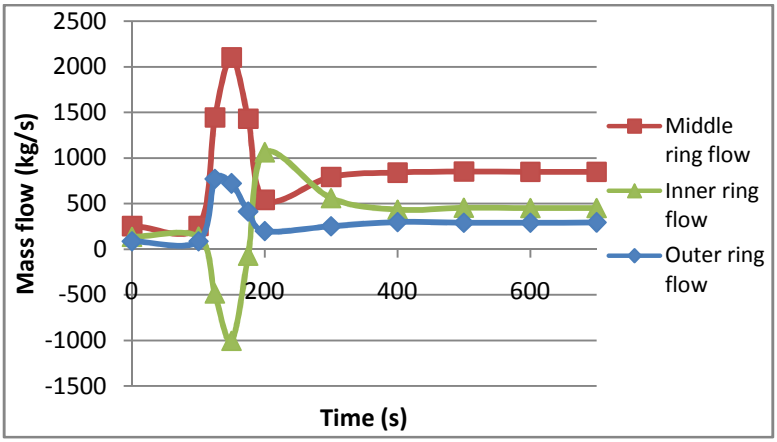

Figure 5.44: Flow in the different rings of the core for $1.0 insertion

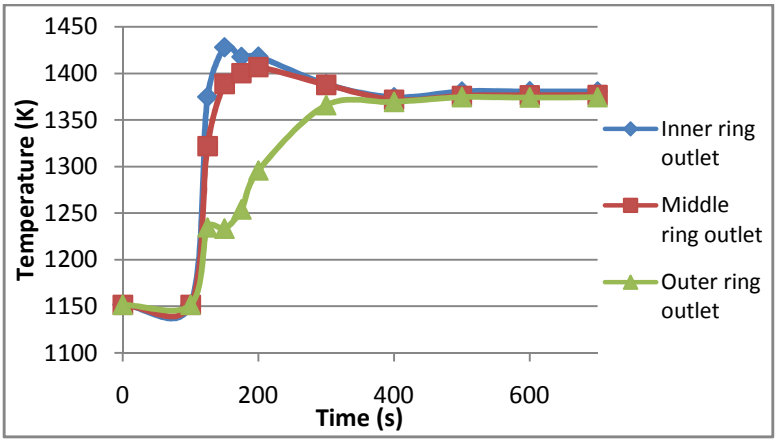

Figure 5.45: Outlet temperature in the different rings of the core for $1.0 insertion

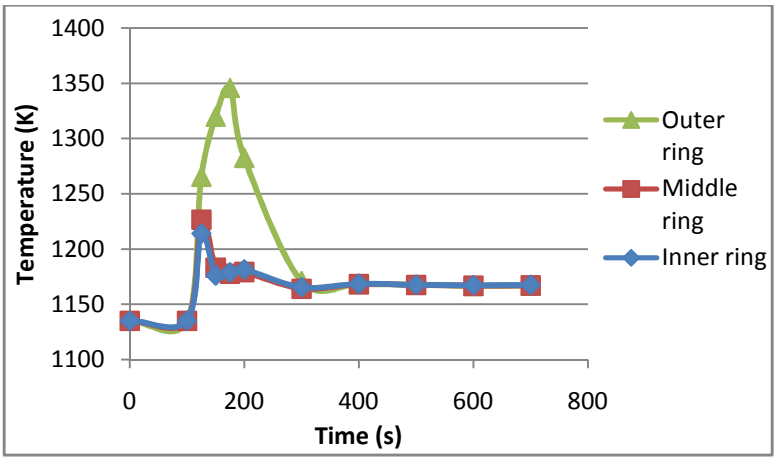

Figure 5.46: Temperature of the first axial segment in the different rings of the core for $1.0 insertion

These figures were added in order to show with more precision the phenomena that occur in the core after the reactivity swing. Figure 5.45 shows that the outlet temperature of the assemblies in the three regions of the core increases after 50 s, but the increase in the outer region is less significant. Indeed, the outlet temperature of the outer region of the core increases from 1135 K at t = 100 s to 1206 K at t = 125 s. In addition, the temperature in the first axial segment of the outer assemblies goes to 1261.7 K, resulting in a negative temperature differential. This negative temperature difference is due to the reverse flow, which may occur because the average temperature (and therefore density) in the outer ring of the core is lower than that in the other rings. This phenomenon is similar to that pointed out in section 5.5.1.2 for the $0.15 reactivity insertion. It was observed that the decrease in the outer ring flow is more significant when the reactivity insertion increases. Thus, an increase of the initial reactivity addition leads to an increase of the amplitude of the unstable effect. A negative flow in the outer region represents an internal loop in the reactor core, with part of the coolant flowing upwards in the inner and middle assemblies, and another part flowing downwards in the outer region. To achieve a stable and optimal start-up of the reactor, one should suppress this type of internal loop phenomenon.

5.5.1.5 $1.5 step reactivity insertion

A simulation was run to study the effect of a $1.5 step reactivity insertion. The results of this simulation are given in Figure 5.47 to Figure 5.53.

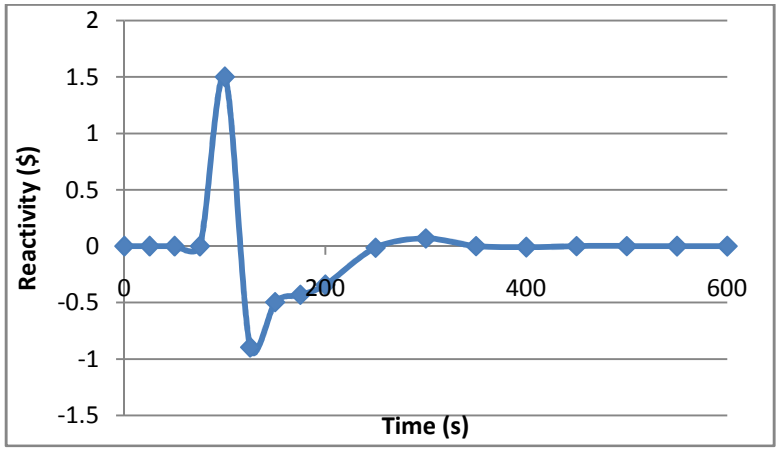

Figure 5.47: Core reactivity changes over time for $1.5 step insertion

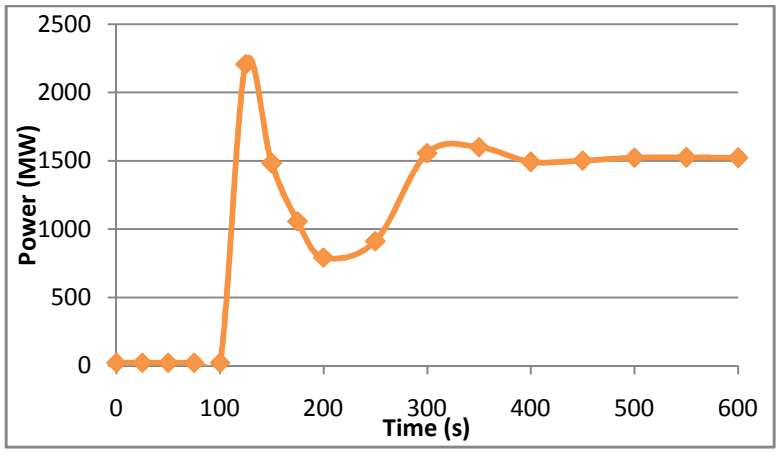

Figure 5.48: Total core power changes over time for $1.5 step insertion

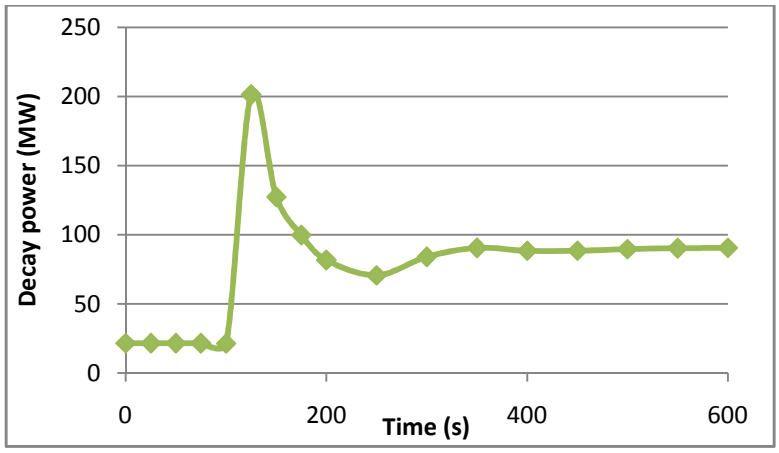

Figure 5.49: Decay power changes over time for $1.5 step insertion

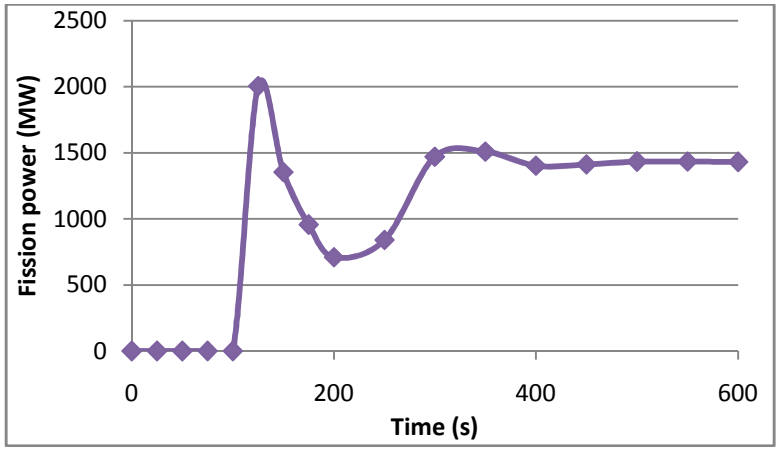

Figure 5.50: Fission power changes over time for $1.5 step insertion

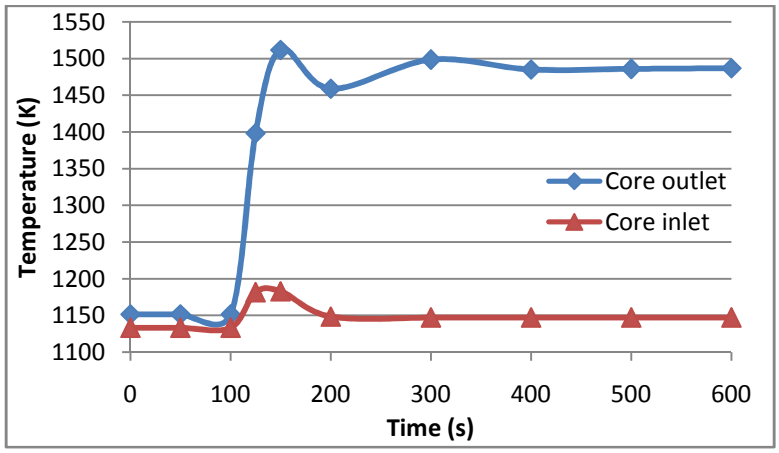

Figure 5.51: Core inlet and outlet temperature changes over time for $1.5 step insertion

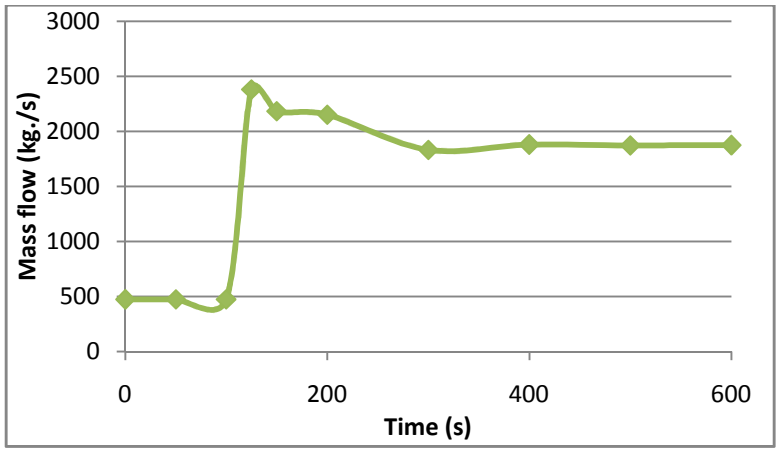

Figure 5.52: Total core mass flow changes over time for $1.5 step insertion

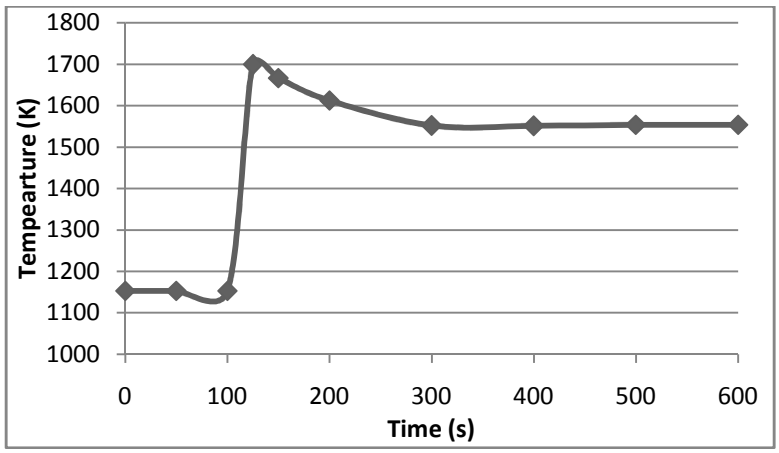

Figure 5.53: Fuel centerline peak temperature in the inner ring changes over time for $1.5 step insertion

For a $1.5 reactivity insertion at time 100 s, the power level is increased to 1520 MW and the total core mass flow 1873.8 kg/s. The core outlet and fuel centerline peak temperatures are 1487.2 and 1554 K. A significant negative flow was observed in the outer region during a portion of the transient. The results of this simulation were presented to show the magnitude of the changes in power and mass flow rate that resulted from inserting a significant (in fact unrealistically high) amount of reactivity. It is observed that when the reactivity insertion goes from $0.15 to $1.5, the total core power achieved at the end of the simulation is increased by 1421.5 MW, and the core mass flow

rate is increased by 1088.1 kg/s. While the reactivity inserted is multiplied by 10, the power achieved is multiplied by 15.4 and the core mass flow rate is multiplied by 2.4.

5.5.1.6 Summary of single step reactivity insertion simulations

The results of eight different single step reactivity insertions are summarized and presented in Table 5.7, and will be discussed in the next section.

Table 5.7: Summary of single step reactivity insertions

Reactivity inserted ($)	Final Power (MW)	Fraction of total power achieved	Peak fuel temperature (K)	Negative flow during transient
0.00	21.5	0.90	1153.2	No
0.10	70.0	2.92	1179.0	No
0.15	98.6	4.11	1191.8	No
0.20	138.2	5.76	1204.4	Yes
0.50	369.2	15.38	1282.7	Yes
1.00	897.3	37.39	1418.0	Yes
1.25	1200.0	50.00	1486.0	Yes
1.50	1521.7	63.40	1554.0	Yes
1.55	1588.0	66.17	1567.7	Yes

5.5.2 Potential start-up procedure

5.5.2.1 Discussion of single step reactivity insertion results

The results presented in the previous section were analyzed to establish limits on the amount of reactivity that could be added by a single step insertion without jeopardizing the stability of the system. Also, the total amount of reactivity that could be inserted by making successive single step reactivity insertions without risk was evaluated.

As discussed in sections 5.2.1.2 and 5.2.1.4, the step insertion of reactivity may induce negative flow in the outer fuel assemblies of the core. In order to proceed to a safe restart of the LS-VHTR, no such phenomenon should be observed. Several simulations were run to determine a limit on the inserted reactivity in order to avoid negative flows. It was found that reactivity insertion less or equal to $0.18 would not induce reverse flow.

Thus, no more than \$0.18 reactivity in one step should be added in order to avoid counter-flow.

The limit on the fuel temperature was also examined. Current coated TRISO fuel particles offer the capability to operate for long periods at temperatures up to 1523 K (1250°C) [2]. Thus, the total amount of reactivity added to the core by successive step reactivity insertion should not make fuel centerline temperatures hotter than 1523 K. Among the simulations presented in section 5.5.1, the fuel centerline temperature goes past this limit in the \$1.5 insertion case. Additional simulations with different amounts of reactivity inserted in the core were run, in order to study the impact of reactivity insertion on the fuel peak temperature. The maximum fuel temperature and the fraction of total power reached at the end of the transient after adding 7 different amounts of reactivity are shown in Figure 5.54.

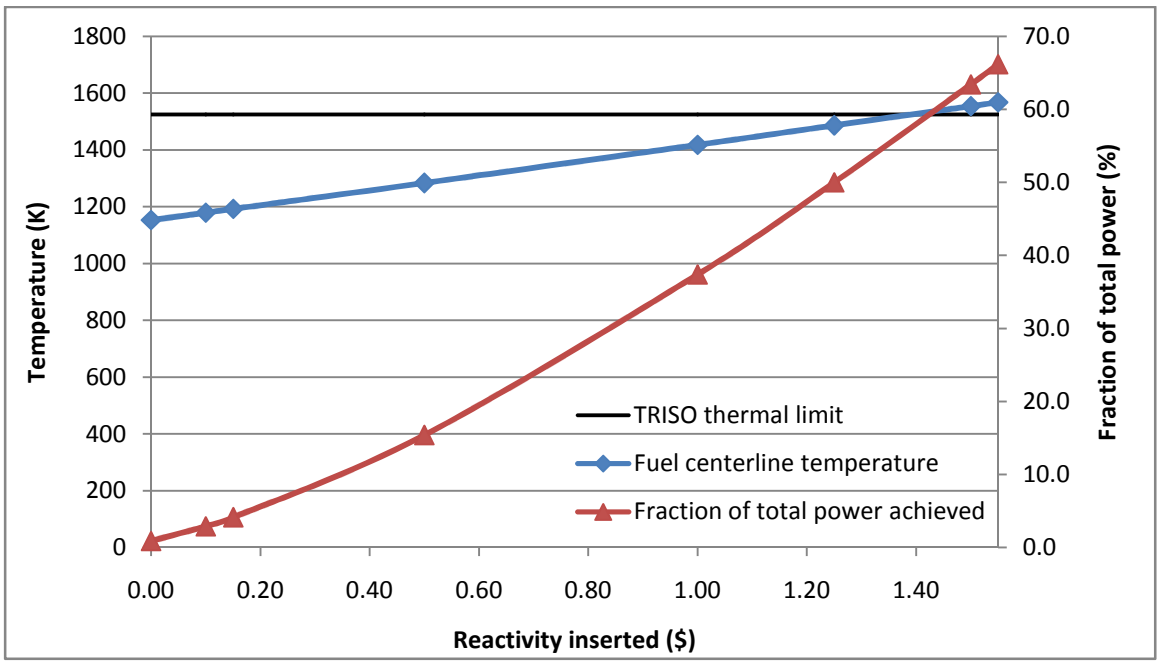

Figure 5.54: Peak fuel centerline temperature and fraction of total power achieved for 7 different step reactivity insertions

The maximum fuel temperature is below the TRISO thermal limit for a \$1.25 insertion and above the limit for a \$1.5 insertion. The fuel centerline temperature curve

intersects the TRISO thermal limit line for inserted reactivity around $1.40. Thus, the amount of a single step reactivity insertion should remain below this value (plus some safety margin) to preserve the integrity of the TRISO fuel particles.

5.5.2.2 Discussion on potential complete start-up procedure and simulation

Given the results presented in section 5.5.1, section 5.5.2.1, and the experience of natural circulation power plant start-ups discussed in section 3.1.2, a potential start-up procedure for the LS-VHTR with natural circulation of the salt coolant was devised.

Figure 3.1.5 in section 3.1.2 shows that the power of the ESBWR during the start-up is increased by step. This is likely due to successive control rod removal at different times during the start-up. Thus, it was decided to define a similar kind of start-up, with successive positive step reactivity insertions.

Based on the discussion made in the previous section, and in order to prevent any type of instability, it was decided to maintain the insertion of positive reactivity below or at $0.15.

As mentioned in section 5.5.2.1, the fuel temperature should not go past 1523 K in order to preserve the integrity of the TRISO fuel. As a consequence, the amount of successive step insertion was chosen so that the maximum fuel temperature in the core does not exceed that value.

The initial reactivity inserted was done at time t = 100 s after the beginning of the simulation. The next insertion was done at time t = 2000 s, and the following insertions were made every 1000 s after this second insertion as shown in Figure 5.55. The total reactivity inserted with this set of eight $0.15 reactivity additions was $1.2.

Figures 5.56 to 5.63 show the behavior of the total core reactivity, core power level, decay and fission power, temperature and flow with respect to time during the simulated start-up of the LS-VHTR.

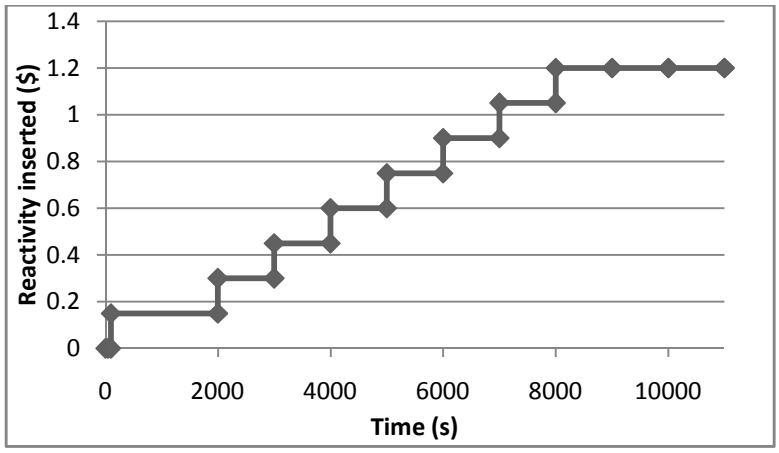

Figure 5.55: Reactivity insertion curve for the start-up simulation

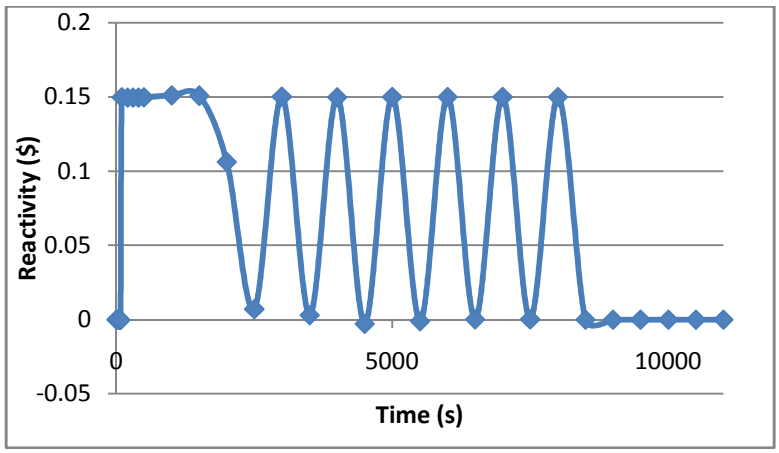

Figure 5.56: Total core reactivity during the start-up

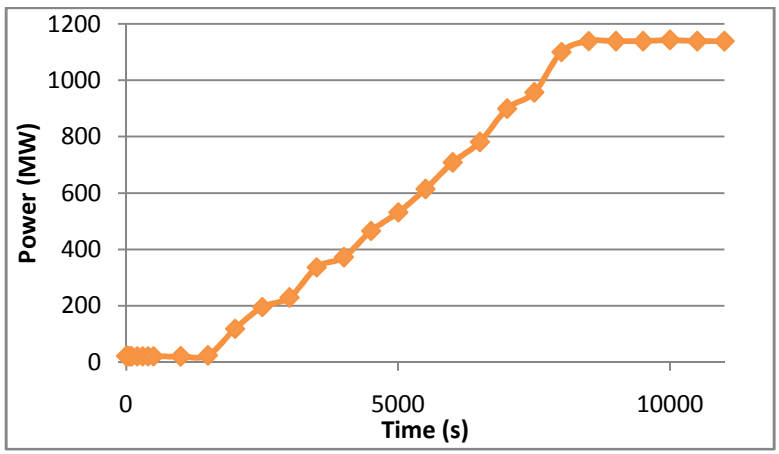

Figure 5.57: Total core power during the start-up

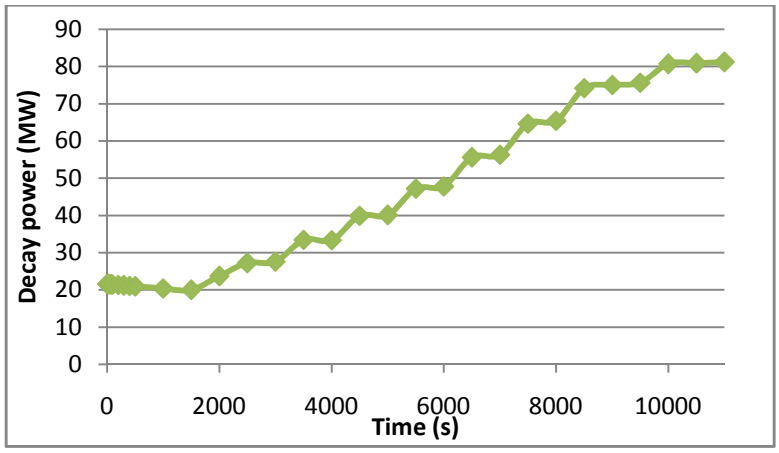

Figure 5.58: Decay power level during the start-up

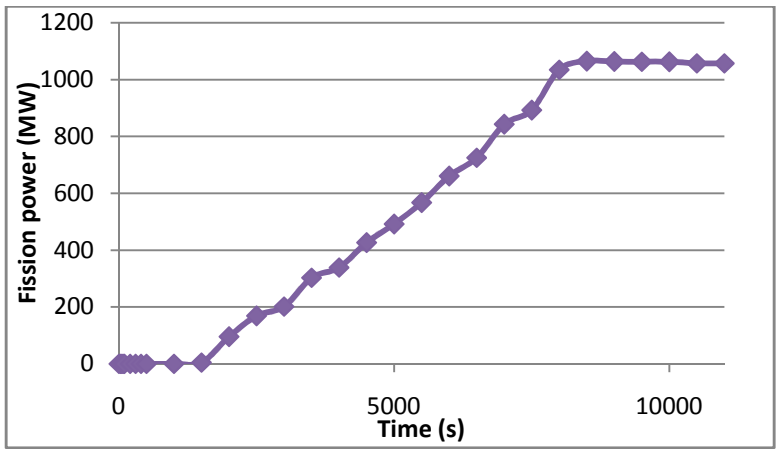

Figure 5.59: Fission power level during the start-up

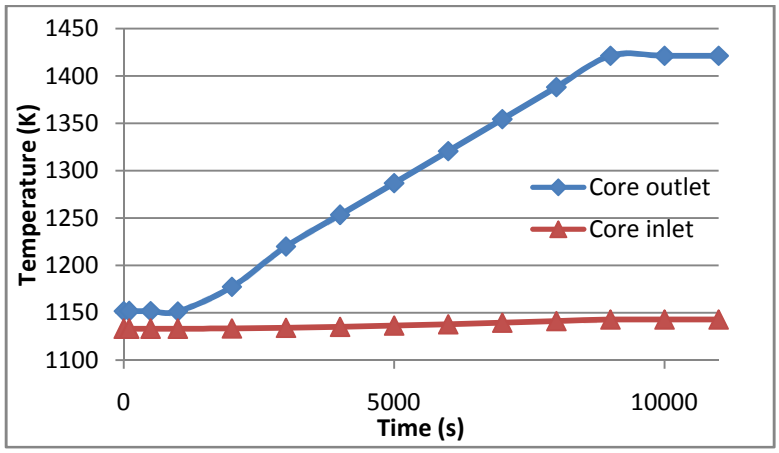

Figure 5.60: Core inlet and outlet temperatures during the start-up

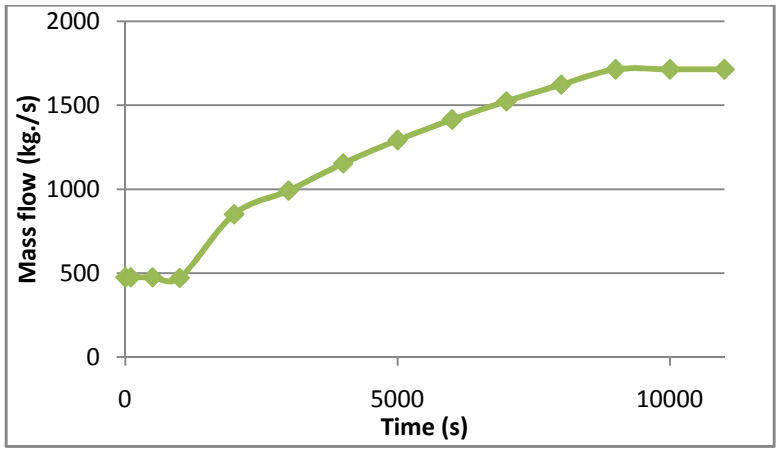

Figure 5.61: Total core mass flow during the start-up

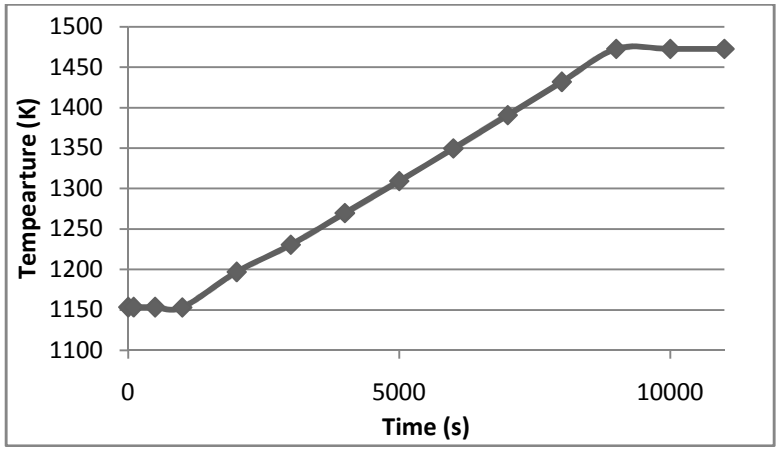

Figure 5.62: Fuel centerline peak temperature during the start-up

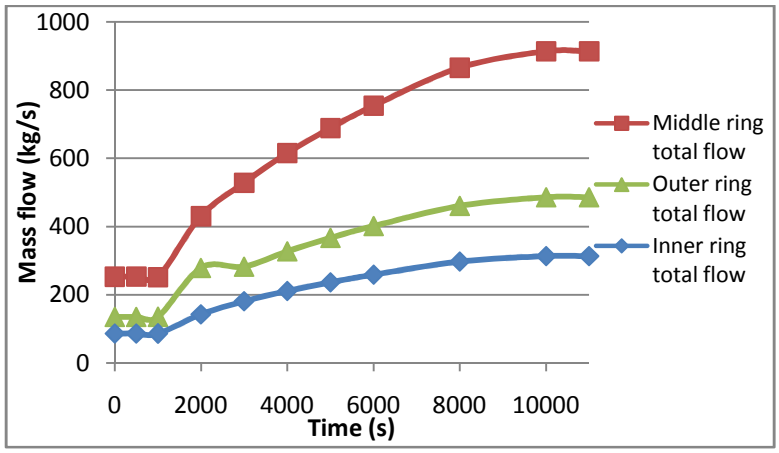

Figure 5.63: Mass flow in the different core regions during the start-up

Figure 5.56 shows that during the start-up, the reactivity oscillates between 0 and some positive values. This is due to the fact that a step of positive reactivity is inserted in the core every time that the total reactivity of the core decreases due to the feedback. No negative flow was observed in the outer ring of assemblies during the simulation. The total core mass flow reaches 1713.2 kg/s at the end of the start-up. This flow corresponds to 17.3% of the core mass flow under full power conditions. The core power level goes from 21.5 MW initially to 1138 MW after 18000 s. Thus, with this set of successive reactivity insertions, it takes 2.5 hours to bring the reactor to 47.5% of the total reactor power level.

The core inlet temperature was increased by 10 K while the core outlet temperature increase is 269.7 K. The maximum fuel temperature during the start-up is achieved at the end of the process, with 1472.5 K. This value is 50 K below the limit for preserving the integrity of the coated particles, thus making this start-up procedure safe regarding fuel temperature.

The results of the start-up simulation showed that no more than 47.5% of the total reactor power level may be reached using natural circulation of the coolant. During the start-up and power increase, it is of course necessary to provide an ultimate heat sink. In order to achieve full power conditions, it is necessary to start generating electricity using the turbines and to restart the circulating pumps at some time during the start-up.

The pumping power required to run the pumps may be calculated using the following equation [38]:

$$P_{pump} = \frac{\Delta P \times V}{0.9}$$

where P_{pump} is the pumping power needed in W, ΔP is the pressure drop in Pa, and V is the volumetric flow rate in m^3/s. The denominator 0.9 is used to account for the pump efficiency. The pumping power needed will increase with time since it is proportional to the mass flow. Though, since the rate of core power increase is greater than the rate of

salt flow increase, at some time after the beginning of the start-up the amount of power generated will be sufficient to provide enough electricity to run the pumps. To estimate this time, one should take into account the power conversion efficiency, calculate the electrical power production capability of the reactor at any time during the start-up, and compare that value to the pumping power needed.

At the end of the start-up simulation presented previously, the thermal power is 1472.5 MW, the core mass flow is 0.95 m^3/s (FLiBe density is assumed to be 1800 kg/m^3), and the pressure drop is 0.2 MPa. Therefore, the calculated pumping power is 233.3 kWe. Using the value of thermal efficiency given in Table 2.4; 0.54, the electrical power generated at the end of the simulation would be 795.15 MWe which is many times more. Thus, the restart of the pumps using the electricity provided by the turbines would be possible.

In real life, power production followed by synchronization to grid would be initiated at much lower power, perhaps 3-5% full power, and the electricity produced would need to provide not only pumping power, but the whole power plant electric needs. However, this was beyond the scope of this study and is left for future research.

CHAPTER 6

CONCLUSIONS AND FUTURE WORK

6.1 Conclusions

Neutronics and thermal-hydraulic performance of a LS-VHTR were examined. The purpose of this study was to develop and analyze a start-up procedure for this reactor with natural circulation of the coolant including LOOP conditions, in order to evaluate its feasibility and stability. A model of the LS-VHTR core was developed using the CSAS6 sequence of the SCALE6.0 package to quantify the reactivity feedback due to changes in the fuel temperature or coolant density. A model of the reactor using ORNL baseline design specifications using the RELAP5 software was also developed to simulate the thermal-hydraulic behavior of the reactor during full power operation, shutdown and start-up, and to determine the core reactivity and power changes during a plant start-up. Simulations were performed to determine a potential start-up procedure for the LS-VHTR with natural convection of the coolant, and then to analyze and evaluate this process.

The neutronic calculations evaluated the negative Doppler coefficient for the reactor under study. It was also shown that a decrease in FLiBe density would lead to a positive reactivity feedback. Besides, it is essential to point out that the change in reactivity induced by the coolant density feedback is negligible compared to the effect of the fuel temperature feedback, thus making the overall reactivity feedback negative and the LS-VHTR passively safe.

Different step reactivity insertion cases were studied, and showed that inserting more than \$0.15 of reactivity in the LS-VHTR core eight hours after its shutdown from full operating conditions could lead to unstable internal coolant loops. In addition, it was shown that inserting more than \$1.2 in the core would make fuel temperatures go past the

thermal capability of the TRISO particles. A potential start-up trajectory was then devised and simulated. The results obtained showed that the reactor power level can be brought to 47.5% of full power without exceeding the fuel thermal limits, and using natural convection of the primary coolant to transfer the heat generated to the intermediate loop.

It should be taken into account that assumptions were made, and the findings presented in this report should be observed with an appropriate distance. The RELAP5 code was initially developed to simulate the behavior of systems with water as the coolant. Even if the properties of FLiBe and FLiNaK were subsequently added, RELAP5 was mainly used to simulate full power conditions operation or shutdown scenario for the LS-VHTR. Simulating the start-up of the LS-VHTR and coupling the thermal hydraulics with the kinetics is novel, and the results obtained with these simulations may slightly differ from what would happen in reality. Thus, this study only provides an indication about the stability and feasibility of a start-up procedure for the LS-VHTR with natural convection of the salt coolant.

For the assumptions used in this work, it was shown that a stable procedure could be developed, as the one presented in section 5.5.2.2, and that a significant core power could be achieved by inserting reactivity stepwise eight hours after the shutdown of the reactor. Thus, this study demonstrated the potential for a passive start-up of the LS-VHTR. However, the work done in this thesis should be taken further in order to get a thorough evaluation of the feasibility of a start-up procedure that would not require any offsite power.

In this study, the thermal-hydraulics modeling focused on the primary loop components. The flow and temperatures in the secondary loop were assumed and entered in the RELAP5 code as boundary conditions. Moreover, the power production loop was not modeled in this study, the power conversion efficiency was assumed based on ORNL expectations for their LS-VHTR conceptual design, and the power needed for the

instrumentation of the plant, for the circulating pumps of the intermediate and power production loop, and for the turbines was not taken into account. To get more realistic results, the modeling of the intermediate loop and of the power production loop should be included in the study. Thus, further work would be needed to provide a more thorough analysis.

6.2 Future work

Future work beyond the scope of this thesis could include calculations of Doppler and density reactivity coefficients for different fuel burnups. In this study, the neutronics calculations were done at the beginning of life of the fuel, and fresh fuel was assumed everywhere in the fuel assembly. Further work could include considering multiple batches with different enrichments in the fuel assembly and in the core.

The axial and radial power distributions were assumed based on results found in literature. To get more precise results, SCALE6.0 could be used to calculate the exact axial and radial power profiles for the LS-VHTR core. Also, further work should include considering the intermediate salt loop and the power production loop in the model in order to fully describe the problem and to take into account the pumping power needed to drive the intermediate salt and power conversion system loop gas flows. Further work should also include the determination of optimal designs for the primary (FLiBe to FLiNaK) and secondary (FLiNaK to supercritical carbon dioxide or helium) heat exchangers. The RELAP5 model could also be improved by including a pump component that would emulate more realistically the behavior of the primary loop circulating pump. Detailed calculations should also be done to determine form loss coefficients, in order to model accurately the friction losses in the primary loop. In addition, some research could be done on how to model realistically the performance of the TRISO fuel in RELAP5.

Finally, further analysis of operating procedure could be done to determine an optimal and detailed start-up procedure. Further work could also include evaluating the possible location and worth of control rods, in order to determine how much reactivity could be inserted by removing some or all of the control rods.

REFERENCES

[1] U.S. DOE Nuclear Energy Reasearch Advisory Committee. "A Technology Roadmap for Generation IV Nuclear Energy Systems Executive Summary", March 2003.

[2] D. T. Ingersoll, C. W. Forsberg, L. J. Ott, D. F. Williams, J. P. Renier, D. F. Wilson, S. J. Ball, L. Reid, W. R. Corwin, G. D. Del Cul, P. F. Peterson, H. Zhao, P. S. Pickard, E. J. Parma, M. Vernon. "Status of Preconceptual Design of the Advanced High-Temperature Reactor (AHTR)", Oak Ridge National Laboratory, ORNL/TM-2004/104, May 2004.

[3] World Nuclear Association. "Nuclear Power in the Netherlands", http://www.world-nuclear.org/info/inf107.html.

[4] U.S. Nuclear Regulatory Commision. "Design certification application reviews - EBWR", http://www.nrc.gov/reactors/new-reactors/design-cert/esbwr/review-schedule.html.

[5] D. F. Hollenbach, J. A. Bucholz. "Theoretical background for calculational methods in SCALE", Oak Ridge National Laboratory, ORNL/TM-2005/39, January 2009.

[6] The RELAP5-3D Code Development Team. "RELAP5-3D© Code manual volume I: code structure, system models, and solution methods", Idaho National Laboratory, INEEL-EXT-98-00834, June 2005.

[7] D. T. Ingersoll, C. W. Forsberg, P. E. MacDonald. "Trade Studies for the Liquid-Salt-Cooled Very High Temperature Reactor: Fiscal Year 2006 Progress Report", Oak Ridge National Laboratory, ORNL/TM-2006/140, February 2007.

[8] M. A. Stawicki. "Benchmarking of the MIT High Temperature Gas-Cooled Reactor TRISO-Coated", MIT, May 2006.

[9] Idaho National Laboratory, INL. "*NGNP Next Generation Nuclear Plant",* http://www.nextgenerationnuclearplant.com/facility/triso-fuel.shtml.

[10] D. T. Ingersoll. "Status of Physics and Safety Analyses for the Liquid-Salt-Cooled Very High-Temperature Reactor (LS-VHTR)", Oak Ridge National Laboratory, ORNL/TM-2005/218, December 2005.

[11] D. F. Williams, L. M. Toth, K. T. Clarno. "Assessment of Candidate Molten Salt for the Advanced High-Temperature Reactor (AHTR)", Oak Ridge National Laboratory, ORNL/TM-2006/12, March 2006.

[12] D. E. Holcomb. “Fluoride Salt Cooled High-Temperature Reactors (FHRs), Successor to the LWR?”, Presentation for Georgia Tech Graduate Seminar, Oak Ridge National Laboratory, January 2011.

[13] L. C. Olson. “Materials Corrosion in Molten LiF-NaF-KF Eutectic Salt”, University of Wisconsin-Madison, 2009.

[14] D. E. Holcomb, F. J. Peretz, A. L. Qualls. “Advanced High Temperature Reactor Systems and Economic Analysis”, Oak Ridge National Laboratory, ORNL/TM-2011/364, September 2011.

[15] H. J. Lin, P. F. Peterson. “Conceptual Design of the Intermediate Heat Exchanger (IHX) for the PB-AHTR”, U.C. Berkeley, May 20, 2009.

[16] H. Padleckas. “Shell-and-tube heat exchanger”, http://en.wikipedia.org/wiki/Shell_and_tube_heat_exchanger, 2006.

[17] M. S. Sohal, M. A. Ebner, P. Sabharwall, P. Sharpe. “Engineering Database of Liquid Salt Thermophysical and Thermochemical Properties”, Idaho National Laboratory, March 2010.

[18] P. K. Vijayan, A. K. Nayak. “Natural Circulation Systems: Advantages and Challenges” Annex 3 of “Natural circulation in water cooled nuclear power plants”, International Atomic Energy Agency, IAEA-TECDOC-1474, November 2005.

[19] C. Kullberg, K. Jone, C. Heath. “Operating Experience of Natural Circulation Core Cooling in Boiling Water Reactors”, Idaho National Engineering Laboratory, 1993.

[20] J. A. Beard. “ESBWR Overview”, GE Hitachi Energy, September 15, 2006.

[21] L. E. Fennern. “ESBWR Seminar - Reactor, Core & Neutronics”, GE Energy, September 15, 2006.

[22] GE Nuclear Energy. “ESBWR Design Control Document”, Tier 2, Chapter 4, Reactor, August 2005.

[23] W. M. Stacey. Nuclear Reactor Physics, WILEY-VCH, Second Edition, 2007.

[24] S. Glasstone, A. Sesonke. “Nuclear Reactor Engineering”, Von Nostrand Reinhold, 1981.

[25] J. J. Duderstadt, L. J. Hamilton. “Nuclear Reactor Analysis”, WILEY Interscience, 1976.

[26] N. E. Todreas, M. S. Kazimi. “Nuclear Systems I, Thermal Hydraulics Fundamentals”, Hemisphere Publishing Corporation, 1990.

[27] S. Goluoglu, D. F. Hollenbach, L. M. Petrie. “CSAS6: control module for enhanced criticality safety analysis with KENO-VI”, Oak Ridge National Laboratory, January 2009.

[28] RSICC. “SCALE code package”, http://www-rsicc.ornl.gov/codes/ccc/ccc7/ccc-750.html.

[29] D. F. Hollenbach, L. M. Petrie, S. Goluoglu, N. F. Landers, M. E. Dunn. “KENO-VI: a general quadratic version of the KENO program”, Oak Ridge National Laboratory, ORNL/TM-2005/39, January 2009.

[30] C. B. Davis. “Implementation of Molten Salt Properties into RELAP5-3D/ATHENA”, Idaho National Laboratory, September 2005.

[31] Haynes International Inc. “HASTELLOY® N alloy”, 2002.

[32] The RELAP5-3D© Code Development Team. “RELAP5-3D© Code Manual Volume II: User’s Guide and Input Requirements / Appendix A RELAP5-3D© Input Data Requirements”, Idaho National Laboratory, INEEL-EXT-98-00834-V2, 2005.

[33] P. E. MacDonald. “NGNP Preliminary Point Design - Results of Initial Neutronics and Thermal-Hydraulic Assessment During FY-03”, Idaho National Engineering and Environmental Laboratory, INEEL/EXT-03-00870, 2003.

[34] ANSI/ANS. “American National Standard for Decay Heat Power in Light Water Reactors”, 1979.

[35] V. E. Schrock. “A Revised ANS Standard for Decay Heat from Fission Products”, Nuclear Technology, 46, pp. 323-331, 1979.

[36] M. Pavlova, P. Groudev, M. Pavlova, P. Groudev, J. Roglans. “RELAP5/MOD3.2 analysis of natural circulation test at Kozloduy NPP unit 6”, Institute for Nuclear

[37] L. Winters. “Assessment of RELAP5/MOD2 against a natural circulation experiment in nuclear power plant Borssele”, International Agreement Report, July 1993.

[38] D. E. Holcomb, D. Ilas, V. K. Varma, A. T. Cisneros, R. P. Kelly, J. C. Gehin. “Core and refueling design studies for the advanced high temperature reactor”, Oak Ridge National Laboratory, ORNL/TM-2011/365, September 2011.